PERGAMON

Journal of Structural Geology 24 (2002) 1431–1450

JOURNAL OF STRUCTURAL GEOLOGY

www.elsevier.com/locate/jstrugeo

On the role of melt-rock reaction in mantle shear zone formation in the Othris Peridotite Massif (Greece)

Arjan H. Dijkstra[a,b,*], Martyn R. Drury[b], Reinoud L.M. Vissers[b], Julie Newman[c]

[a]*Department of Geology, University of Leicester, LE1 7RH, Leicester, UK*
[b]*Veining Meinesz School of Geodynamics, Universiteit Utrecht, Utrecht, The Netherlands*
[c]*Department of Geology and Geophysics, Texas A&M University, College Station, TX, USA*

Received 19 January 2001; accepted 1 November 2001

Abstract

A 1-km-wide peridotite mylonite shear zone is exposed in the Othris peridotite massif in central Greece. The mylonites contain lenses of relatively coarse olivine crystals, which are interpreted as remnants of the tectonite microstructure in the adjacent wall rocks. Microstructure and texture analysis using light and SEM microscopy suggests that the dominant deformation mechanism in the tectonites was dislocation creep, whereas the deformation in the mylonites was probably controlled by grain-size sensitive (GSS) creep in fine-grained (<50 μm) bands consisting of a mixture of olivine and orthopyroxene. The development of the fine-grained material in the mylonites can be explained by a melt-present reaction taking place in the tectonite protolith. This reaction led to the replacement of orthopyroxene porphyroclasts by fine-grained olivine and orthopyroxene. Tectonites adjacent to the mylonite zone preserve evidence for this reaction in the form of rims of fine-grained olivine and orthopyroxene around orthopyroxene porphyroclasts. This study illustrates the significance of rheological weakening of oceanic mantle lithosphere as a result of a change from dislocation to GSS creep.

Keywords: Peridotite mylonite; Peridotite tectonite; Melt-rock reaction; Shear localisation; Ophiolite; Microstructures

1. Introduction

1.1. Peridotite mylonite shear zones

Mylonite shear zones are commonly found in peridotite massifs (e.g. Boudier et al., 1988; Ceuleneer et al., 1988; Vissers et al., 1991; Hoogerduijn Strating et al., 1993; Furusho and Kanagawa, 1999; Newman et al., 1999) and in peridotites recovered from the ocean floor (e.g. Jaroslow et al., 1996). Peridotite mylonites may control the strength of the mantle lithosphere (e.g. Vissers et al., 1995, 1997), and therefore play a crucial role in lithosphere-scale deformation processes such as continental rifting or mountain building. Peridotite mylonites in the oceanic lithosphere are responsible for exhumation of mantle rocks to the ocean floor at mid-ocean ridges, in particular in slow-spreading oceans (e.g. Cannat, 1993; Jaroslow et al., 1996). Moreover, peridotite mylonites are commonly involved in the detachment of ophiolite massifs from their oceanic environment and in their subsequent emplacement onto the continents (e.g. Boudier et al., 1988). Despite the fact that peridotite mylonites play an important role in tectonics, the processes associated with their formation—in particular grain size reduction—are still poorly understood. On the basis of a detailed microstructural study of a well-developed and excellently exposed peridotite mylonite zone in the Othris peridotite massif in central Greece, we conclude that grain size reduction combined with mixing of mineral phases, both as a result of (melt-rock) reactions, provides an important mechanism for weakening and strain localisation in mantle rocks.

1.2. Strain localisation and weakening

Shear localisation, i.e. the formation of shear zones, can occur in materials under various conditions. In materials exhibiting elastic, elastic-brittle, or pressure-sensitive elastic-plastic deformation, a shear localisation instability can be initiated during strain softening, steady-state deformation, or strain hardening (Hobbs et al., 1990). For materials like olivine, in which plastic deformation is largely pressure-insensitive, some sort of weakening is probably required for shear localisation. Moreover, for

* Corresponding author. Correspondence address: Department of Geology, University of Leicester, University Road, Leicester, LE1 7RH, UK.
E-mail address: ahd3@le.ac.uk (A.H. Dijkstra).

0191-8141/02/$ - see front matter
PII: S0191-8141(01)00142-0

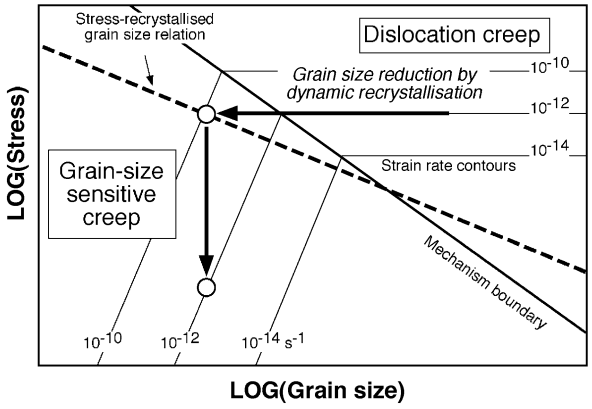

Fig. 1. Schematic deformation mechanism map for olivine (based on figure 9 of Rutter and Brodie, 1988). Thick line is the mechanism boundary between the dislocation and grain-size sensitive (GSS) creep fields. Thick dashed line shows the empirical relation between the stress and the recrystallised grain size. Thick arrows show weakening effect of grain size reduction by dynamic recrystallisation: the weakening effect can be an increase of the strain rate at constant stress (horizontal arrow), a decrease of stress at constant strain rate (vertical arrow), or a combination of both. It is, however, questionable whether dynamic recrystallisation can bring a rock into the GSS creep field (see text).

deformation to remain localised in a shear zone, the material inside the shear zone has to be significantly weaker than the surrounding material, otherwise the zone of localised deformation widens and the shear zone becomes a self-arresting instability (e.g. Poirier, 1980; White et al., 1980; Hobbs et al., 1990; Rutter, 1999). Therefore, rheological weakening of the material inside a shear zone with respect to the material outside the shear zone is required to explain the occurrence of large shear zones in natural rocks, even if such shear zones have been formed in a system that was hardening with time. The processes that could cause significant weakening in natural rocks (White and Knipe, 1978; Poirier, 1980; White et al., 1980), and peridotites in particular (Drury et al., 1991), are thermal weakening, geometric weakening, reaction weakening, chemical weakening, melt weakening, and a change of the dominant deformation mechanism. For a review of the relative importance of each of these processes in peridotites under mantle conditions the reader is referred to Drury et al. (1991). The most drastic weakening effect at sub-solidus conditions is produced by a change from dislocation to grain-size sensitive (GSS) creep. GSS creep, which comprises a combination of diffusion creep and grain boundary sliding, occurs at low deviatoric stresses in fine-grained rocks. Many microstructural studies of natural peridotite mylonites conclude that this process is responsible for localisation of deformation in peridotite mylonite zones (Boullier and Gueguen, 1975; Drury et al., 1990; Vissers et al., 1995; Jaroslow et al., 1996; Jin et al., 1998; Furusho and Kanagawa, 1999; Newman et al., 1999).

Questions remain, however, as to the processes that cause the transition from dislocation to GSS creep in peridotites. It has been proposed that dynamic recrystallisation during dislocation creep deformation can lead to grain size reduction, which in turn promotes GSS creep (Fig. 1; Twiss, 1977; White et al., 1980; Rutter and Brodie, 1988; Karato and Wu, 1993; Jaroslow et al., 1996). However, as dynamic recrystallisation only takes place during dislocation creep, it remains uncertain whether dynamic recrystallisation can bring a rock fully into the GSS creep regime (e.g. Etheridge and Wilkie, 1979; De Bresser et al., 1998). It is therefore important to investigate alternative mechanisms by which the grain size in a rock can be reduced, and, at least as important, how the small grain size can be stabilised. Detailed studies by Newman et al. (1999) and Furusho and Kanagawa (1999) have shown that the nucleation of new small grains by a metamorphic reaction in peridotites could account for extreme grain size reduction and formation of peridotite mylonites. In this paper it is argued that melt-rock reactions can have a similar effect.

1.3. Methods

In this study we carried out structural mapping in the field followed by detailed microstructural analysis of peridotite tectonite and mylonite samples. We used an integrated approach, combining light microscopy, scanning electron microscopy (SEM), fabric analysis by means of a universal stage (U-stage) mounted on a light microscope and SEM electron backscatter diffraction (EBSD), and thermometry based on chemical analyses obtained with an electron microprobe. All microstructural observations presented below have been made on thin sections prepared parallel to the lineation and perpendicular to the foliation as determined in outcrop.

SEM backscatter and secondary electron images were obtained using a Philips XL30FEG (field emission gun) scanning electron microprobe at the Utrecht University Centre for Electron Microscopy (EMSA), operating at 15–25 kV. Samples consisted of standard polished thin sections, which were subjected to additional chemical polishing for a few hours using a Syton suspension. Olivine and pyroxene grains can be distinguished by their relief as a result of this polishing technique: olivine crystals show a positive relief whereas pyroxenes show negative relief. Additional SEM images were obtained using the forward scattering configuration with the sample tilted 70° with respect to the electron beam (Prior et al., 1996, 1999). Individual grains can be recognised by their orientation contrast in such images (Prior et al., 1996; Fliervoet et al., 1999). Lattice orientation of small crystals (generally $<$0.1 mm) were determined by means of the SEM–EBSD technique (Randle, 1992; Fliervoet et al., 1999; Prior et al., 1999).

Grain sizes were determined using a linear intercept method, counting the number of grain intersections (several hundreds) on lines parallel and perpendicular to the foliation, using orientation contrast SEM images (for

fine-grained bands) and polarised-light microscope photomosaics (for coarse-grained lenses).

Chemical analyses of mineral grains for pyroxene geothermometry were obtained using a Cameca SX-50 electron microprobe at the Geology and Geophysics Department of Texas A&M University (USA) with wavelength dispersive spectrometers equipped with LiF, PET and TAP crystals. Operating conditions comprised an acceleration voltage of 15 kV, a 10 nA beam current, and element counting times of 20–60 s. Chemical analyses were taken on profiles across porphyroclasts, carefully avoiding cracks, inclusions, and exsolutions, using a relatively large 15–20 μm spotsize. Analyses on fine-grained mineral phases were obtained using a smaller spotsize of 5–10 μm.

1.4. The Othris Peridotite Massif

The Othris Peridotite Massif constitutes the mantle section of the dismembered Tethyan Othris Ophiolite (Menzies, 1973, 1976; Menzies and Allen, 1974; Rassios and Konstantopoulou, 1993), which probably originated in a near-transform environment at a slow-spreading ridge (Dijkstra et al., 2001). A kilometre-wide peridotite mylonite zone is well exposed along the Onohonos River in the Katáchloron area (Fig. 2). This shear zone and several smaller mylonite zones cut across peridotite tectonites. As shown below, the tectonites, in particular those on the eastern side of the large mylonite zone, can be considered as the protolith of the mylonites, and will also be discussed in detail. The mylonite shear zones in Othris are formed in a compressional or transpressional setting, probably related to the first stages of emplacement of the Othris Ophiolite (Dijkstra, 2001).

2. The Othris peridotite mylonites and tectonites

2.1. The mylonites

The harzburgites in the kilometre-wide, near-vertical N–S striking Onohonos River mylonite zone (Fig. 2) exhibit a strong foliation and lineation caused by flattened and stretched pyroxenes and bands or augen-shaped domains of fine-grained material around pyroxenes. Lineations have sub-horizontal to moderately steep south-plunging orientations. Mylonitic harzburgites are interleaved by metre to 10-metre scale dunite bands and lenses, which enclose pyroxene-bearing enclaves. The dunites locally contain bands or clusters of black (chrome-rich) spinel. Within the mylonites thin, 1–10-cm-wide dunite bands are often boudinaged or sometimes broken up into small, relatively angular fragments.

At several locations, the N–S striking mylonites are cross-cut by oblique mylonite to ultramylonite zones, which are generally a few centimetres wide but which are occasionally as wide as >50 m (Fig. 2). We reserve the term ultramylonite for mylonites that have a vitreous appearance in the field due to a high proportion of very fine-grained material. Cross-cutting mylonites and ultramylonites are not restricted to the Onohonos River mylonite zone; they are occasionally found within the adjacent harzburgite and plagioclase–peridotite domains. They are generally steeply NE-dipping, striking NW–SE; some are sub-vertical striking NE–SW. Trails of small spinel grains define south-plunging lineations. A reverse, sinistral plus E-up sense of movement was established from the progressive rotation of older foliations into the thin NW–SE striking (ultra-)mylonite zones.

A large fault-bound block of plagioclase-bearing mylonites is found on the southern slope of Mt Katáchloron (Fig. 2). At this location, N–S striking mylonites are cross-cut by numerous, thin, NW–SE and NE–SW striking mylonites to ultramylonites. Plagioclase is also present in adjacent tectonites and its crystallisation from an impregnating melt pre-dates the formation of the mylonites (Dijkstra et al., 2001).

2.2. The peridotites of the western block

The peridotites occuring west of the Onohonos River mylonite zone (further referred to as the western block) are coarse-grained harzburgite tectonites. The coarse-grained appearance is mainly caused by the presence of numerous large orthopyroxene porphyroclasts, which are typically 5–15 mm in diameter. The orthopyroxene clasts generally do not produce a strong foliation or lineation. Occasionally flattened and elongated spinel define a foliation and lineation. More commonly, a well-defined compositional layering defined by variations in modal orthopyroxene content is observed. It was confirmed in places that the layering and the foliation are sub-parallel, striking N–S to NE–SW with a steep down-dip lineation.

Large, 10 to 100-metre-scale dunite bodies occur within the tectonites of the western block. They generally strike NE–SW and cross-cut the harzburgite tectonite fabric. These dunites consist almost entirely of (serpentinised) olivine. Occasional spinel form centimetre-scale clusters, sometimes with a core of strongly altered orthopyroxene.

The transition from the coarse tectonites to the mylonites is well-defined. One coarse tectonite–mylonite transition exposed in the banks of the Onohonos River has been mapped in detail (Fig. 2). In the transition zone, numerous relatively thin mylonite zones cross-cut the coarse tectonite foliation. They are mostly found at the margins of large dunites. In these mylonite zones the orthopyroxene crystals are elongate and their size is reduced as compared with the orthopyroxenes in the tectonite protolith. Towards the east, the mylonitic zones become wider until no more coarse tectonites are found. The width of the dunite bodies within the mylonites is strongly reduced to several tens of metres to a few centimetres.

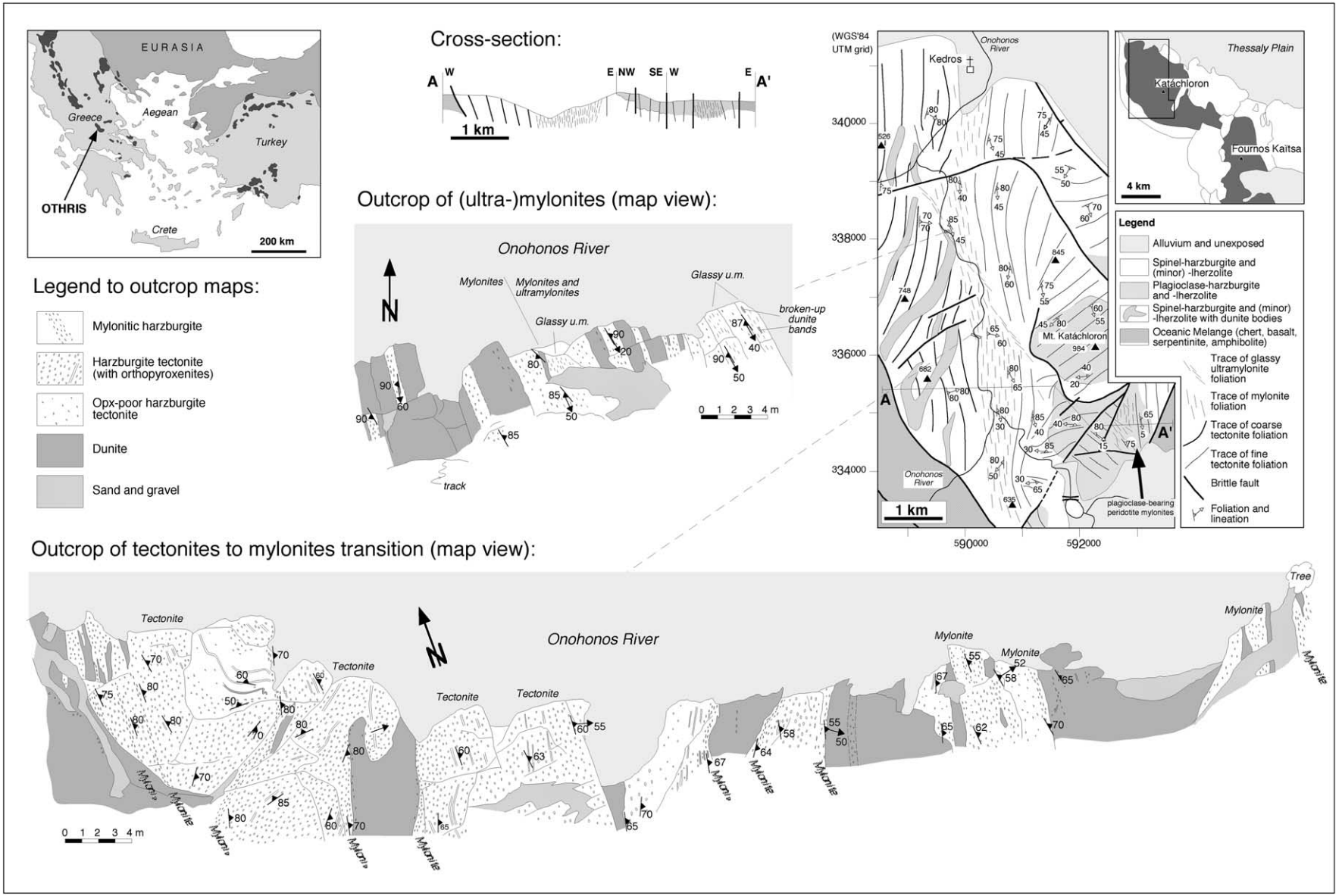

Fig. 2. Geological maps, cross-sections, and outcrop maps showing location of Othris peridotite massif in Greece (inset at upper left), structure of the Katáchloron area with location of cross-section A–A′ (inset at upper right—outline of dunite bodies after unpublished geological map; A. Rassios, personal communication, 1995); section across the Onohonos mylonites zone (middle top). Also shown are two detailed outcrop maps showing the transition of coarse-grained tectonites to mylonites (lower part of page) and a band of vitreous ultramylonites within the mylonite zone (middle).

2.3. The peridotites of the eastern block

The peridotites east of the Onohonos River mylonite zone, referred to here as the eastern block, are predominantly fine-grained harzburgite tectonites with few, small dunites. Orthopyroxene crystals are mostly small, less than 6 mm in diameter, and they are surrounded by light-coloured rims of fine-grained polyphase material. The fine-grained tectonites are moderately well foliated; typically, however, they are strongly lineated. Lineations and foliations are defined by flattened and stretched orthopyroxene, olivine, spinel, and fine-grained polyphase rims around orthopyroxene porphyroclasts. Locally, the fine-grained tectonites contain orthopyroxene-, spinel-, and olivine-rich layers. This compositional layering is generally parallel to the tectonite foliation. At a few locations, isoclinally folded layers were found with axial planes parallel to the foliation. Moreover, some strongly boudinaged websterite bands occur. At two locations, small 10–50 cm size, irregular dunites have been found, which cross-cut the tectonite foliation and compositional layering. The harzburgite tectonites adjacent to the Onohonos River mylonite zone are structurally continuous with plagioclase–harzburgites and plagioclase–lherzolites, which occur on the top and the southern and northeastern slopes of Mt Katáchloron. From the foliation pattern, it is evident that deformation recorded in the fine-grained harzburgite tectonites flanking the mylonite zone overprints the deformation in the plagioclase–peridotites towards the east, since NE–SW to E–W striking foliations in the plagioclase–peridotites bend into the N–S striking foliations of the harzburgite tectonites directly adjacent to the mylonite zone. Fine-grained tectonites very similar to those of the eastern block (including plagioclase-bearing tectonites) are also found in the Fournos Kaĭtsa Massif (see small inset map in upper right corner of Fig. 2 for location).

In contrast to the relatively sharp transition from the coarse tectonites to the mylonites in the western block, the transition from fine-grained tectonites to mylonites is gradual in the eastern block. Close to the main mylonite shear zone, orthopyroxene crystals and the fine-grained rims around orthopyroxene in particular are increasingly stretched and flattened, and they eventually coalesce and form continuous fine-grained bands within the mylonite zone.

3. Microstructures and lattice fabrics

3.1. Microstructures in mylonites and ultramylonites

Typical peridotite mylonites consist of polyphase bands of fine-grained olivine, orthopyroxene, and minor clinopyroxene and spinel. The fine-grained polyphase bands enclose markedly coarser bands and lenses consisting almost entirely of olivine (Fig. 3a). The mylonites and ultramylonites cross-cutting the main mylonite zone have broadly similar microstructures, but with higher proportions of fine-grained polyphase material. Some ultramylonites display a fluidal texture (Fig. 3b).

The olivine crystals in the fine-grained polyphase bands are generally smaller than 50 μm in size, down to a few microns. The grains are generally slightly elongate (aspect ratios <3) parallel to the mylonite foliation. A mean linear intercept grain size of 11 μm (LOG grain size 1.02 ± 0.186) was determined from SEM orientation contrast images (e.g. Fig. 3c). It is difficult, however, to distinguish subgrains from grains in such images since the orientation contrast between two areas in the image is not a measure of the angular difference in lattice orientation. The determined linear intercept grain size of 11 μm may therefore be an underestimation of the actual grain size.

The fine-grained bands contain numerous grain boundary alignments parallel or at a small angle (<30°) to the mylonite foliation. These grain boundary alignments can be seen by light microscopy (Fig. 3d) as well as by SEM (Fig. 3c). They often separate bands of different grain sizes, and can be traced over distances of about a millimetre at most before they die out within domains of fine-grained matrix material.

The coarse olivine bands and lenses have a porphyroclastic microstructure with relatively few olivine porphyroclasts. The mean linear intercept grain size of the coarse bands is 121 μm (LOG grain size 2.134 ± 1.333), determined from polarised light microscope photo-mosaics. Olivine porphyroclasts can be a few millimetres in size; they often have a sub-structure of subgrain walls oriented at a high angle to the mylonite foliation. Crystal orientation measurements show that these subgrain walls are mostly parallel to the (100) plane. Some porphyroclasts contain a mesh consisting of two sets of closely spaced irregular subgrain walls or deformation bands, one subparallel to the foliation (parallel to the (001) plane and one at high angles to the foliation (parallel to the (100) plane). The smaller grains usually show little or no sub-structure. Although the coarse bands are mainly mono-mineralic, they contain small grains of orthopyroxene in interstices or as narrow tapering crystals along olivine grain boundaries.

Occasionally, parts of the coarse bands and lenses have an annealed appearance. Such domains have a granular texture with 120° triple junctions, in which the olivine crystals are relatively coarse, ~0.5–1 mm (Fig. 3e). The olivine grain boundaries are free of orthopyroxene, in contrast to the grain boundaries of the adjacent irregular and much smaller olivine grains (Fig. 3e and f).

The mylonites contain orthopyroxene, and occasionally olivine, clinopyroxene and spinel porphyroclasts, mainly within fine-grained bands. Some of the orthopyroxene porphyroclasts are strongly stretched. In one ultramylonitic sample, stretched orthopyroxene porphyroclasts are broken up into smaller fragments, and an assemblage of fibrous tremolite and chlorite occurs in the spaces between the fragments (Fig. 3g). Mylonites that developed within plagioclase-bearing peridotites contain porphyroclasts of plagioclase in the fine-grained polyphase matrix (Fig. 3h).

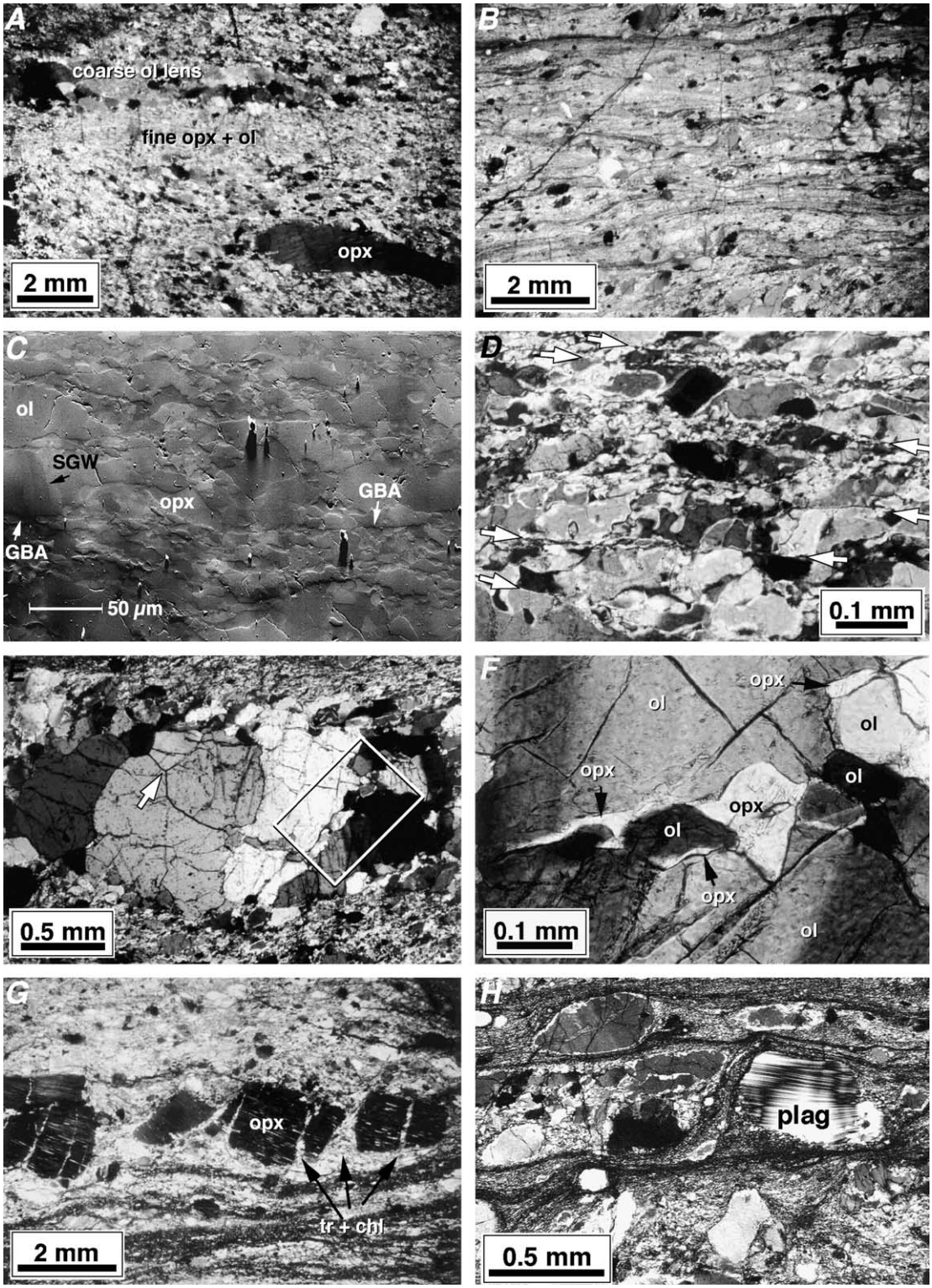

3.2. Microstructures in the coarse tectonites from the western block

The microstructures of the coarse tectonites of the western block are characterised by coarse, 1–3 mm olivine porphyroclasts surrounded by smaller (0.1–0.7 mm) olivine grains (Fig. 4a). The olivine porphyroclasts have highly irregular grain outlines, in contrast to the smaller grains, which have more regular to polygonal, equant shapes. The olivine porphyroclasts can be elongate (aspect ratios generally less than two), but the elongation direction is variable and can be at a high angle to the tectonite foliation. The

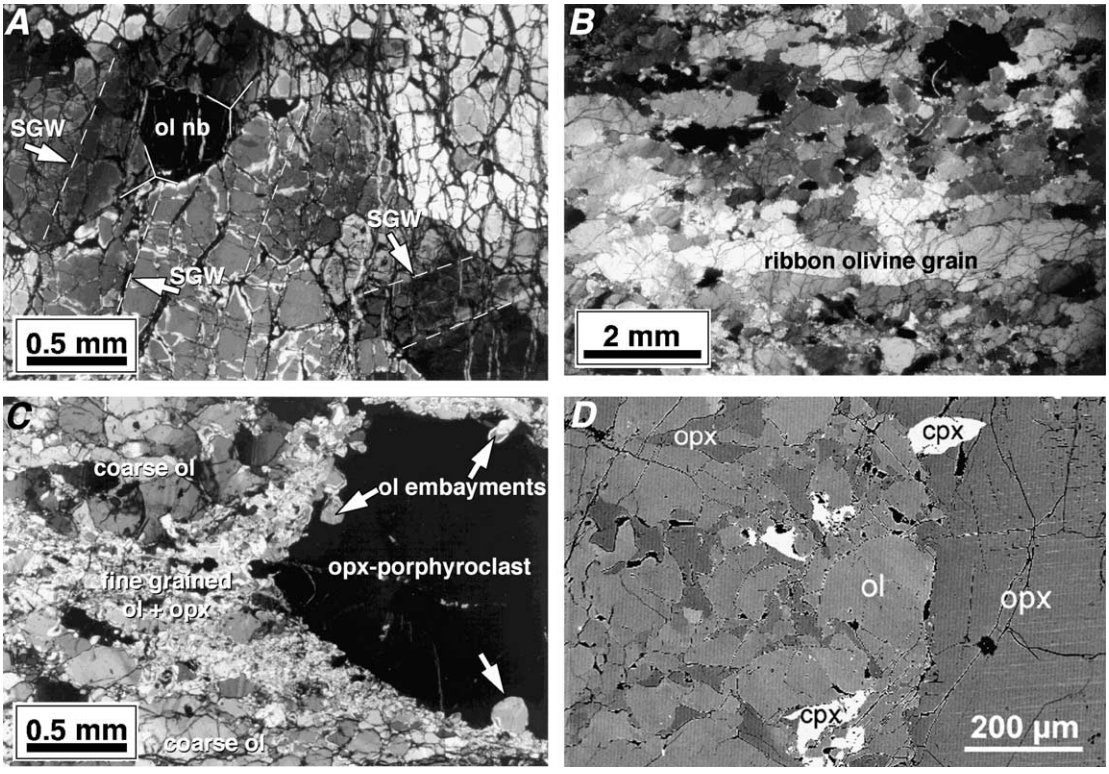

Fig. 4. Micrographs of tectonites. (A) Close-up of coarse tectonite microstructure (XPL) from western block, showing polygonal olivine neoblast ('ol nb') surrounded by olivine porphyroclasts. White arrows indicate subgrain walls (SGW) in olivine porphyroclasts. (B) Photomicrograph (XPL) of a typical olivine-rich domain from a fine tectonite from the eastern block containing elongate, ribbon-like olivine grains. (C) Photomicrograph (XPL) showing fine-grained olivine–orthopyroxene mixture in an augen-shaped domain around orthopyroxene porphyroclast (at extinction), interpreted as product of melt-present breakdown reaction of orthopyroxene (see text for discussion). (D) Backscatter SEM image showing mineralogy and texture of a fine-grained domain adjacent to an orthopyroxene porphyroclast.

foliation is defined by stretched spinel grains, by trails of spinel grains, and by bands of olivine neoblasts. The olivine porphyroclasts have a sub-structure of (100) subgrain walls at a high angle to the foliation, whereas the smaller grains do not seem to have a well-developed sub-structure.

The coarse tectonites contain syn-kinematic pargasitic hornblende occurring together with orthopyroxene, clinopyroxene, and aluminous spinel in coarse corona-like rims around orthopyroxene porphyroclasts. They also contain late-stage, post-kinematic tremolitic amphibole, which overgrows the tectonite foliation and partially replaces large orthopyroxene crystals.

3.3. Microstructures in the fine tectonites from the eastern block

The tectonites of the eastern block contain two types of microstructural domains: (1) relatively coarse-grained domains of predominantly olivine and trace amounts of orthopyroxene and spinel, and (2) much finer-grained domains consisting of a mixture of roughly equal modal proportions of olivine and orthopyroxene with minor clinopyroxene and spinel.

The coarse-grained, olivine-rich domains have porphyroclastic microstructures, with fewer and smaller olivine

Fig. 3. Micrographs of mylonitic microstructures. (A) Photomicrograph in cross-polarised light (XPL) of typical mylonite, showing fine-grained bands made up of a mixture of olivine and orthopyroxene, and lenses of relatively coarse-grained olivine. Note strongly stretched orthopyroxene porphyroclast in lower right corner. (B) Photomicrograph (XPL) of very fine-grained, fluidal ultramylonite containing porphyroclasts of olivine, orthopyroxene, and spinel. (C) Forescatter SEM image of ultramylonite. Olivine grains have positive relief, orthopyroxene grains show negative relief. Variations in crystallographic orientation cause contrast variations within and among grains (see for instance the subgrain wall (SGW) in relatively large olivine grain in middle left). Note distinct grain boundary alignment (GBA)—interpreted as a sliding surface—between relatively coarse and fine bands in lower half of image. (D) Photomicrograph (XPL) of grain boundary alignments (indicated by white arrows) in a fine-grained olivine–orthopyroxene band in a mylonite. (E) Evidence for local grain growth/annealing in a relatively coarse olivine lens in an ultramylonite (XPL). The granular grains are much coarser than average and display near-perfect 120° triple grain junction. (F) Close-up of area in rectangle (XPL), showing small orthopyroxene crystals along olivine grain boundaries. (G) Broken-up orthopyroxene porphyroclast in ultramylonite (XPL), with fibrous tremolite and chlorite grown in spaces between the orthopyroxene fragments. (H) Plagioclase-bearing mylonite (XPL). Note the flow of the fine-grained polyphase matrix around the plagioclase clast, suggesting that the plagioclase crystal is strong as compared with the matrix.

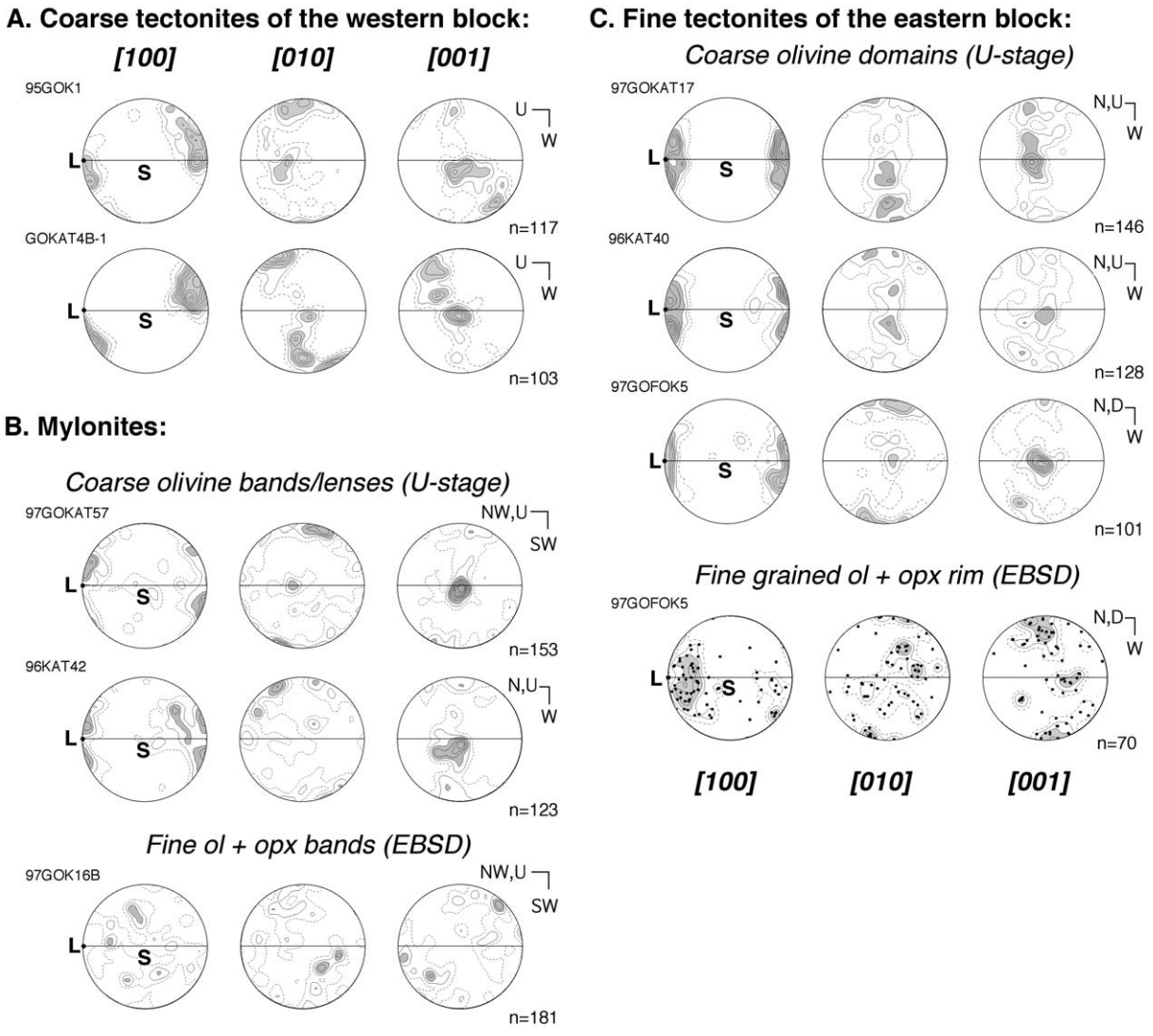

Fig. 5. Lattice preferred orientation (LPO) patterns of olivine from (A) Othris coarse tectonites from western block, (B) mylonites, and (C) fine-tectonites from eastern block, determined by U-stage and SEM–EBSD; lower hemisphere, equal area projections. Horizontal lines in stereoplots denote orientations of tectonite or mylonite foliation (S) in each sample; lineation (L) oriented on the perimeter of each plot; orientation symbols on right of each set of LPO data indicate orientation of stereoplot in geographic co-ordinates (U = up, D = down). Data contoured at 1,2,3,… times uniform.

porphyroclasts as compared with the coarse porphyroclastic tectonites in the western block. A striking aspect of the microstructures of the fine tectonites of the eastern block is the strong elongation of the olivine porphyroclasts (e.g. Fig. 4b); aspect ratios are generally larger than two, and some ribbon olivines occur with aspect ratios as high as 15. Olivine porphyroclasts often have a well-developed sub-structure consisting of (100) subgrain walls generally at a high angle to the foliation. As in the mylonites, many of the olivine porphyroclasts with [*c*]-axes approximately in the plane of section show a second set of (001) subgrain walls sub-parallel to the foliation. Neoblasts have similar to slightly smaller sizes (0.1–0.5 mm) compared with the neoblasts in the coarse tectonites of the western block. No strong sub-structure in the newly recrystallised grains has been observed by light microscopy.

The fine-grained domains occur as rounded or augen-shaped rims around orthopyroxene porphyroclasts (Fig. 4c). These fine-grained domains consist mainly of intermixed olivine and orthopyroxene with minor amounts of clinopyroxene and spinel (Fig. 4d), with grain sizes of 0.2 mm to ~5 μm. Olivine grains in the fine-grained domains do not show a well-developed sub-structure.

3.4. Olivine lattice preferred orientations

Olivine lattice preferred orientations (LPO) in several mylonites and tectonites were determined using a U-stage. Additional LPO measurements of fine-grained olivine in two samples were obtained using the SEM–EBSD technique.

Olivine crystals in two coarse tectonites of the western block have asymmetric LPOs (Fig. 5a). Olivine [*a*]-axes

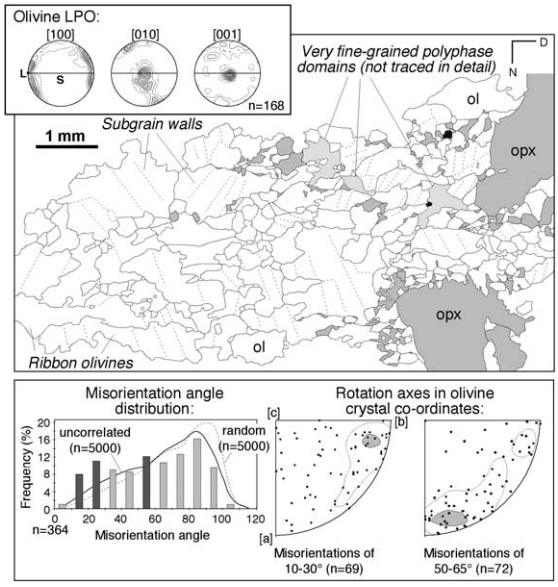

Fig. 6. Detailed microstructural analysis of selected domain of a fine-grained tectonite from the eastern block (sample 97GOKAT16). Inset at top left shows lattice preferred orientation of olivine grains in the domain, determined by U-stage. Main panel shows tracing of a photomosaic of the domain, with orientations of visible subgrain walls in olivine grains indicated by dashed lines. Lower panel shows results of a misorientation analysis. The distribution of misorientation angles between neighbouring grains is compared with the distribution of misorientation angles between pairs of non-neighbouring grains from the sample ('uncorrelated'), and with the calculated distribution of misorientation angles between pairs of grains from a hypothetical sample with a random fabric ('random'). Significantly more misorientations between 10 and 30° and between 50 and 60° occur than expected from the fabric alone. Olivine inverse pole figures in right-hand-side of lower panel show orientations of rotation axes of grain-pairs with 10–30° and 50–65° misorientations, contoured at one and two times uniform distribution.

cluster at a small angle to the lineation, [*b*]-axes form a girdle at a high angle to the foliation, and [*c*]-axes lie within the foliation plane at a high angle to the lineation. These patterns suggest that the dominant slip system in olivine was [*a*] (010), with minor slip on the [*a*] (001) system. The LPO asymmetries of both samples indicate an east-up sense of shear.

Olivine crystal orientations in coarse olivine bands and lenses in two mylonites were measured with the U-stage; three to four individual coarse bands were measured in each sample. The crystals in the coarse bands exhibit an LPO (Fig. 5b) with [*a*]-axes clustering around the lineation orientation and with [*b*]-axes at a high angle to the mylonite foliation, in accordance with slip on the [*a*] (010) slip system. Some [*c*]-axes are oriented at a high angle to the foliation as well, indicating a contribution from the [*a*] (001) slip system to the deformation. The LPOs of the two investigated samples are both asymmetric, suggesting dominant non-coaxial deformation. The asymmetry of the [*b*]-maximum with respect to the foliation in one of the mylonitic samples shown (97GOKAT57) suggests a dextral sense of shear, whereas that of the other mylonitic sample (96KAT42) points to an oblique sinistral plus east-up sense of shear. Note that the [*a*]-axes show double maxima on either side of the lineation orientation. LPO asymmetries of individual bands within samples vary, with different bands yielding opposite senses of shear. Importantly, olivine crystals in several fine-grained bands in one mylonite sample exhibit only a weak LPO (Fig. 5b).

In Fig. 5c, the LPOs are shown for coarse olivine domains in three fine-grained tectonites from the eastern block (determined by U-stage). For one sample (97GOFOK5) olivine crystal orientations in a fine-grained rim around an orthopyroxene porphyroclast (determined by EBSD) are also shown. In general, [*a*]-axes have a preferred orientation near the lineation. Olivine [*b*]- and [*c*]-axes form girdles at a high angle to the lineation. These LPO patterns indicate that slip occurred on the [*a*] {0kl} slip system. In most samples, the LPOs are symmetric or only slightly asymmetric. The few asymmetric fabrics suggest a sinistral plus (south)east-up sense of shear. Olivine in the fine-grained rim exhibits an LPO that is roughly similar to the bulk LPO of olivines from coarse bands in the same sample indicating [*a*] {0kl} slip, although the number of grains is relatively small.

In order to study the role of recrystallisation in the development of the microstructure of the fine-grained tectonites, a detailed misorientation analysis was carried out on a coarse olivine domain from a fine tectonite (Fig. 6). Angles between the crystal lattices of adjacent grains ('misorientations') as well as rotation axes were calculated from the measured crystal orientations (Randle, 1992; Wheeler et al., 2001). If neighbouring grains are derived from a larger olivine crystal by subgrain rotation recrystallisation, relatively small misorientations are expected. In this case, the orientations of the rotation axes give additional information about the types of dislocations involved in the recrystallisation process. The misorientation angle distribution in Fig. 6 shows that grain boundaries with small misorientations are found significantly more frequently than expected from the LPO alone, indicating that subgrain rotation recrystallisation has been an important process in the development of the microstructure. Rotation angles of low angle boundaries have a preferred orientation close to the olivine [*b*]-axes. In addition, slightly more boundaries with misorientations between 50 and 60° are found than expected from the LPO alone. The rotation axes of such boundaries have a small preference for orientations near the [*a*]-axis. Rotations of ~60° around the olivine [*a*]-axis are in accordance with a twinning system in olivine ('t Hart, 1978a).

3.5. Orthopyroxene textures and microstructures

In the peridotites studied from the Othris massif, four morphologically different types of orthopyroxene crystals have been recognised (Figs. 7–9):

1. Large (>0.5 mm) porphyroclasts, generally with exsolution lamellae of clinopyroxene along the cleavage, and

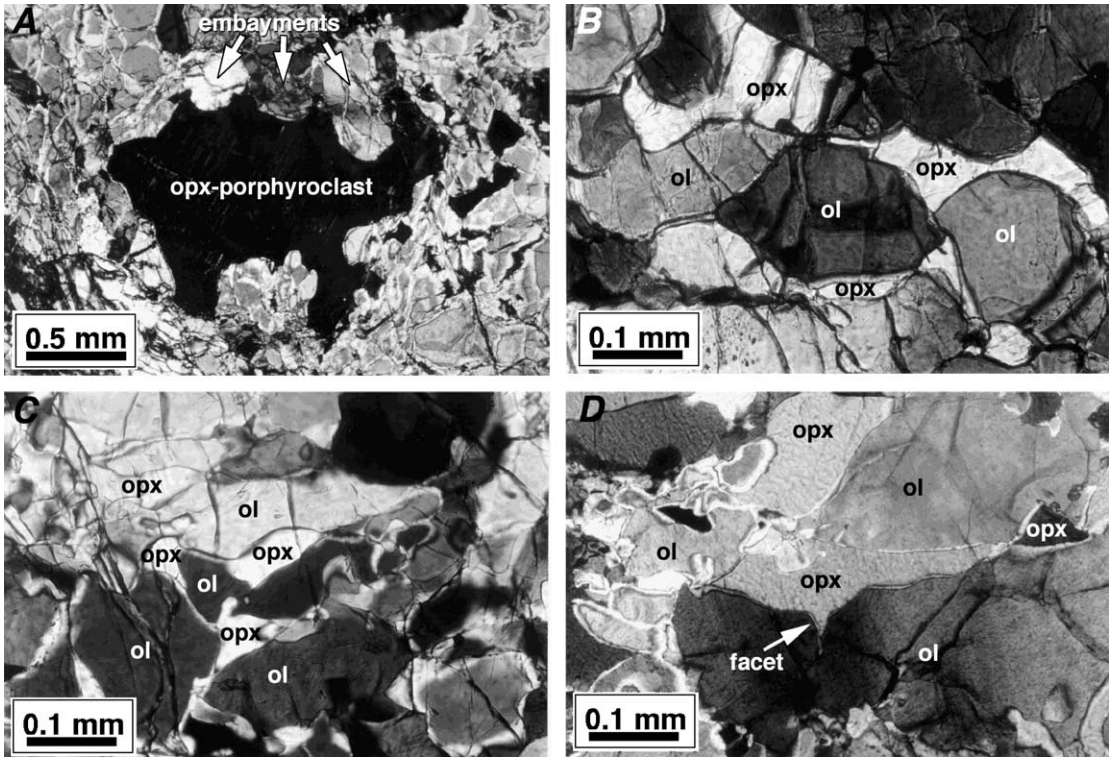

Fig. 7. Micrographs of typical orthopyroxene morphologies. (A) Type-I orthopyroxene porphyroclasts with irregular outline caused by olivine embayments (XPL). (B) Type-II cluster of interstitial orthopyroxene grains, all with the same crystallographic orientations (XPL). (C) Close-up of fine-grained olivine–orthopyroxene domain in fine-grained tectonite containing type-III interstitial orthopyroxene (XPL). (D) Type-IV interstitial orthopyroxene grain in a coarse, olivine domain in a fine-grained tectonite from eastern block (XPL). Note that lower olivine grain has developed a straight crystal face ('facet') at the interphase boundary with the interstitial orthopyroxene grain. Note also sharp, wedge-shaped protrusion of the orthopyroxene grain following orientation of a prominent set of subgrain walls in lower olivine grain.

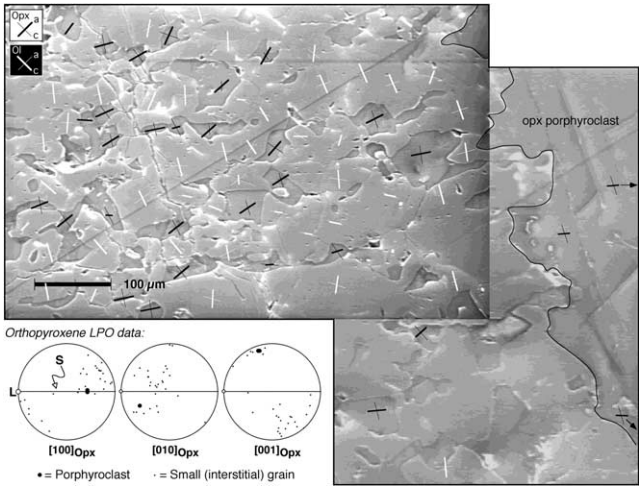

Fig. 8. Secondary electron SEM image of fine-grained olivine–orthopyroxene domain next to an orthopyroxene porphyroclast in a fine-grained tectonite (sample 97GOFOK5). Crystal orientations of olivine and orthopyroxene grains determined by EBSD. Orientations of [*a*]- and [*c*]-axes are shown by projected short lines of uniform length (black for orthopyroxene, white for olivine). Stereoplots (equal area) of orthopyroxene crystal orientations shown in lower left. Orthopyroxene grains have lattice preferred orientations unrelated to any known slip system in orthopyroxene but probably inherited from adjacent orthopyroxene porphyroclast. For olivine LPO of this sample see stereoplots in Fig. 5c.

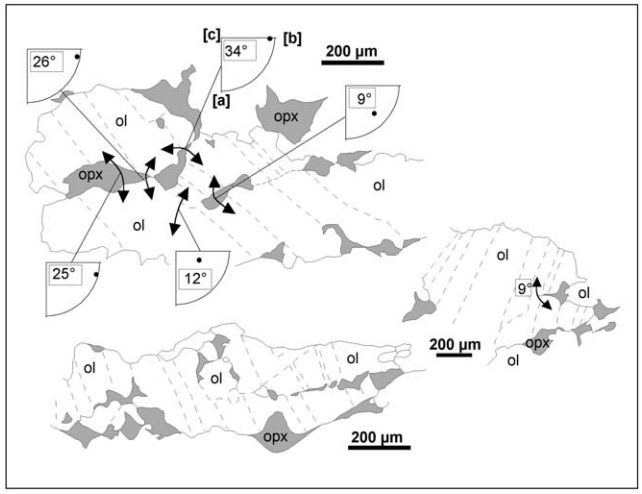

Fig. 9. Tracings from microphotographs showing several (type-IV) orthopyroxene grains distributed along low-angle grain and subgrain boundaries in olivine clusters within coarse olivine-rich domains in fine-grained tectonites. Also shown are the misorientation angles between neighbouring olivine (sub)grains separated by interstitial orthopyroxene grains (measured by U-stage). Inserted inverse pole figures show rotation angles between adjacent (sub)grain pairs. Orthopyroxene is interpreted to be derived by local precipitation from a melt or by replacement of olivine within recrystallising olivine crystals (see text).

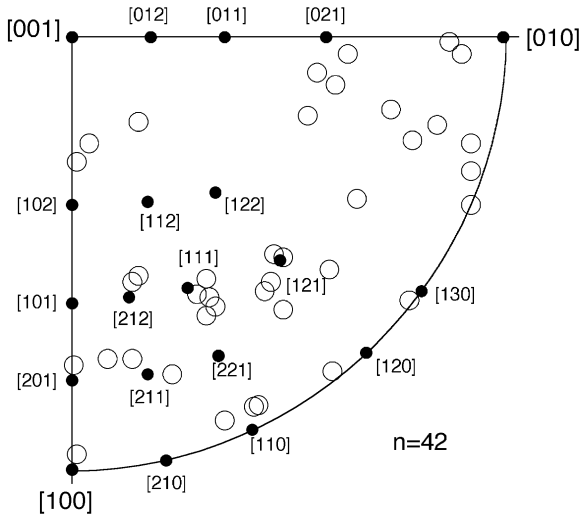

Fig. 10. Inverse pole figure for olivine showing measured orientations (open circles) of the poles to straight olivine faces ('facets') next to interstitial orthopyroxene grains. Orientations were determined in a U-stage by measuring the orientation of the host crystal, and by tilting the facet to a vertical position such as to measure the orientation of the pole to the facet plane. Black dots indicate orientations of poles to low-index olivine crystal planes.

sometimes with spinel exsolutions, are found in all tectonites and mylonites. Such orthopyroxene porphyroclasts often have irregular grain outlines (Fig. 7a), in particular in the coarse tectonites of the western block, but also in domains of coarse plagioclase-bearing tectonites of the eastern block. The irregular grain shape is caused by numerous embayments consisting of olivine and occasionally spinel crystals bulging into orthopyroxene porphyroclasts, which in some cases leads to orthopyroxenes with skeletal shapes. Orthopyroxene clasts of this type are referred to as type-I clasts below.

2. Patches of intermixed olivine and orthopyroxene are found in which the orthopyroxene grains have an interstitial texture. In many cases the orthopyroxene grains seem not to be connected in thin section, yet the individual grains shown simultaneous extinction (Fig. 7b). Such clusters of crystals sharing a common orientation ('orientation family' clusters, referred to as type-II orthopyroxene below) are predominantly found in the coarse-grained tectonites of the western block.
3. In the fine-grained tectonites of the eastern block, orthopyroxene and olivine occur mixed together in fine-grained domains surrounding orthopyroxene porphyroclasts. The same association of mixed orthopyroxene and olivine is found in the fine-grained bands in the mylonites (Figs. 4d and 7c). In this mixture orthopyroxene often has an interstitial or flaser-like shape (type-III orthopyroxene). In the SEM image of a fine-grained domain studied in detail (Fig. 8) olivine and orthopyroxene lattice orientations are indicated by short lines (determined by EBSD). Olivine crystals have orientations that are in agreement with the bulk fabric of the sample, suggesting the activity of the [*a*] {0kl} slip system. The small orthopyroxene crystals also have a lattice preferred orientation, but this preferred orientation bears no relationship with that expected for the known [*c*] (100) or [*c*] (010) slip systems in orthopyroxene. The crystal orientations of the small orthopyroxene crystals are similar to the orientation of the adjacent orthopyroxene porphyroclast.
4. Finally, small amounts of orthopyroxene are found in the relatively coarse olivine-rich domains of the fine-grained tectonites and in the mylonites (type-IV orthopyroxene). Orthopyroxene in these domains occurs as elongate, tapering, flaser-like crystals along olivine grain boundaries aligned sub-parallel to the foliation. Occasionally, such orthopyroxene crystals have developed 'bulges' into adjacent olivines, often following subgrain walls in the olivine crystal. In addition, orthopyroxene crystals occur along low-angle olivine grain boundaries, i.e. grain boundaries between olivine crystals whose lattices are only rotated over small to moderate angles (mostly $<30°$) with respect to each other (Fig. 9). While most olivine–orthopyroxene interphase boundaries are curved, olivine crystals next to typical interstitial orthopyroxene crystals in the coarse olivine domains occasionally have straight crystal faces ('facets'; Fig. 7d). Facets were found to be oriented at high angles to the (001) plane of the host olivine (Fig. 10). Despite considerable scatter, there is a weak preference for orientations near the olivine (111), (121), (110) and possibly the (021) planes. In addition, several facets have poles at a small angle to—but never exactly coinciding with—the [*b*]-axis of the host crystal.

4. Mineral chemistry

4.1. Analytical results

Pyroxene porphyroclasts, analysed by electron microprobe for the purpose of geothermometry, are chemically zoned. Profiles were measured across orthopyroxene and clinopyroxene porphyroclasts in one mylonite and one fine-tectonite sample. The Al concentrations in orthopyroxene decrease from core to rim, whereas Ca concentrations are relatively constant throughout the orthopyroxene grains, and decrease only slightly towards the rim. In clinopyroxene, Al concentrations generally decrease towards the rim and Ca concentrations in clinopyroxene decrease towards the rim.

Fine-grained orthopyroxene and clinopyroxene crystals are also chemically zoned. This is not only observed in

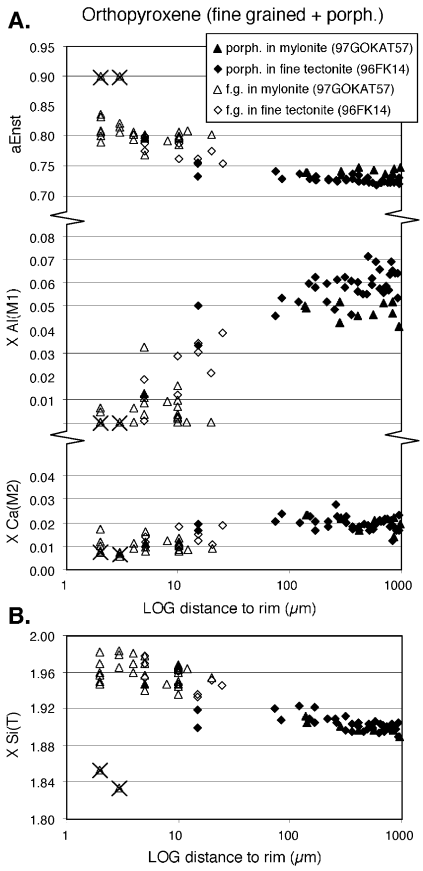

Fig. 11. Chemical data from pyroxene crystals. (A) Chemical profiles of enstatite activity, Al mole fraction in the M1-site and Ca mole fraction in the M2-site as a function of distance between the grain perimeter and the analysis spot, in porphyroclasts and fine-grained orthopyroxene crystals in a mylonite and a fine-grained tectonite. (B) Si mole fraction in orthopyroxene T-site. Crossed points discarded, because the analyses probably included neighbouring olivine grains.

multiple analyses within individual crystals, but also when element concentrations are plotted against (the logarithm of the) distance of the centre of the analysis spot to the grain rim (Fig. 11a); concentrations form a linear array of decreasing Al and Ca from core to rim. The decrease of Al and Ca concentrations towards grain rims is not the result of an unwanted 'mixing in' of olivine (analyses close to the rim are subject to an increased chance that the electron beam partially overlaps with olivine grains adjacent to or underneath the target grain). The effect of a possible contribution of adjacent olivine grains to the analytical results would be to decrease the Si concentration, whilst Fig. 11b shows that the decrease of Al and Ca is associated with an increase in Si towards the rim. The decrease is not the result of exsolution of clinopyroxene either: clinopyroxene exsolution lamellae are restricted to the cores of the orthopyroxene porphyroclasts. The observed chemical trends therefore represent true chemical zonation in the grains. Only two analyses plot at markedly lower Si concentrations, presumably as a result of the discussed mixing effect, and have been discarded.

5. Discussion

5.1. Deformation and recrystallisation in the tectonites

The olivine LPOs, the sub-structures of olivine porphyroclasts, and the evidence for dynamic recrystallisation involving subgrain rotation in the tectonites on either side of the Onohonos mylonite zone all suggest that dislocation creep was the main mechanism in the tectonites controlling deformation and microstructure development, with [*a*] (010) and [*a*] {0kl} as the main slip systems. Many of the studied fine-grained tectonites have weakly asymmetric to symmetric LPOs, indicating either dominantly co-axial strain, or a large non-coaxial strain (i.e. so large a non-coaxial strain that the LPO approaches symmetry with respect to the foliation and lineation). The presence of subgrain boundaries parallel to (001) in addition to the more common (100) subgrain boundaries in olivine porphyroclasts suggests that dislocations with a [*c*]-Burgers vector played a role during subgrain development and contributed to the deformation. Subgrain rotation involving (001) boundaries would have produced new grain boundaries perpendicular to the foliation and parallel to the lineation in tectonites with [*c*]-axis maxima such as in Fig. 6, or parallel to the lineation in samples with [*c*]-axis girdles such as in Fig. 5c. Recrystallisation involving (001) subgrain boundaries can thus (partly) explain the strongly linear character of many fine-grained tectonites.

The misorientation analysis of one fine tectonite sample illustrated in Fig. 6 shows that many of the grain boundaries, which possibly developed from subgrain boundaries by subgrain rotation, are characterised by lattice rotations with rotation axes close to [*b*]. Such rotations can be produced by the transformation of (100) or (001) subgrain walls into grain boundaries by subgrain rotation. The olivine slip systems that could produce such subgrain walls are [*a*] (001) and [*c*] (100), respectively. Both systems are in agreement with the observed (100) and (001) subgrain walls in olivine porphyroclasts. The bulk LPO of the olivine grains indicate that [*a*] (010) was the slip system that contributed most to the deformation of the fine-grained tectonites. Combined slip on all three systems may thus have led to dominant elongation of olivine grains in the lineation direction plus some flattening of the grains.

5.2. Stress estimates

We used empirically derived stress-recrystallised grain size relations for olivine to estimate the differential stress during deformation (Nicolas and Poirier, 1976; Twiss, 1977; Ross et al., 1980). We used the calibration of Van der Wal et al. (1993), which applies to olivine with relatively low water contents. Recently, simple shear deformation experiments on olivine by Zhang and co-workers (2000) have produced markedly smaller grain sizes than those predicted by the Van der Wal et al. (1993) paleopiezometer (Fig. 12). The

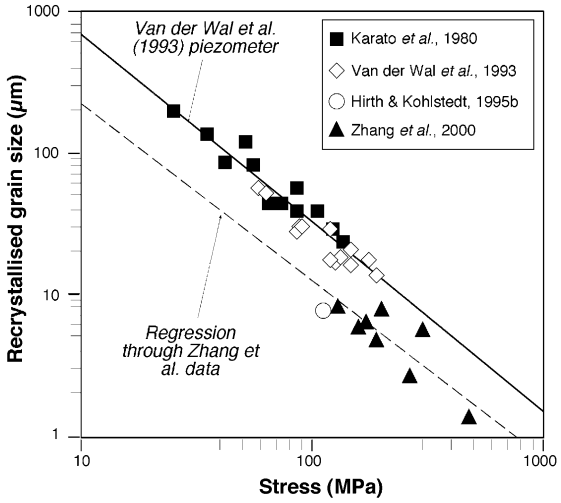

Fig. 12. Summary of available experimentally determined stress-recrystallised grain size data for olivine. Note that data of Zhang et al. (2000) and of Hirth and Kohlstedt (1995b) are at variance with the data from Karato et al. (1980) and Van der Wal et al. (1993). Upper and lower stress estimates derived from the recrystallised grain sizes in Othris tectonites are based on the regressions through the data-sets shown in this diagram.

reported recrystallised grain size in an experiment by Hirth and Kohlstedt (1995b) also deviates from the Van der Wal et al. (1993) relationship and is in agreement with the limited data set of Zhang et al. (2000). A regression through the data of Zhang et al. (2000) was used to obtain a minimum stress estimate, and the Van der Wal et al. (1993) paleopiezometer was applied to obtain a maximum stress estimate from recrystallised grain sizes in the Othris peridotites (Fig. 12). As the data set on which the Van der Wal et al. (1993) relationship is based extends to the relatively low stresses (in the order of a few tens of MPa's) relevant for the Othris peridotites (see below), the Van der Wal et al. (1993) paleopiezometer is considered most appropriate for this study. A correction factor of 1.2 was used to convert the mean linear intercept recrystallised grain size in thin section to a three-dimensional grain diameter. The recrystallised grain sizes of 0.1–0.7 mm in the coarse tectonites correspond to stresses of the order of 3–38 MPa. Similarly, the recrystallised grain sizes of 0.1–0.5 mm in the olivine bands in the fine tectonites yield stresses of 5–38 MPa.

The grain size of olivine in the fine-grained domains is probably not related to the stress through the stress-grain size relations discussed above. As the development of the fine-grained domains was coeval with the deformation and recrystallisation in the coarse olivine bands (as shown by the augen-shapes of the domains), the stresses obtained from the recrystallised grain size in the coarse olivine bands must also be a measure of the stress in the fine-grained domains. The relatively small grain sizes in the polyphase domains suggest that the olivine in the fine-grained domains was not simply produced by dynamic stress-controlled recrystallisation.

5.3. Orthopyroxene textures and the origin of the fine-grained polyphase domains

Irregular orthopyroxene porphyroclast outlines (type-I orthopyroxene), suggesting replacement of orthopyroxene by olivine, are common in harzburgitic mantle sections of ophiolites (see for instance Boudier and Nicolas, 1995). They can be interpreted as products of in-situ incongruent melting of orthopyroxene, which produces olivine and a SiO_2-rich melt (e.g. Niu, 1997). Alternatively, they could be the result of the reaction with an upward migrating melt percolating through the harzburgite. Kelemen (1990) and Kelemen et al. (1992) showed that a basaltic melt becomes undersaturated in orthopyroxene when it moves to shallower levels and thus tends to dissolve orthopyroxene crystals present in the host peridotite. Fluids may also cause incongruent dissolution of orthopyroxene. The coarse-grained tectonites of the western block and some plagioclase-bearing tectonites from the eastern block contain small amounts of (synkinematic) amphibole, showing that the deformation in the tectonites did not occur at temperatures above the stability of amphibole. However, irregular orthopyroxene crystals also occur in peridotites, such as the fine-grained tectonites, which do not show any signs of water-bearing minerals. On the other hand, there is abundant evidence that percolating melts played a prominent role in the formation of the Othris peridotites (Dijkstra et al., 2001). The presence of large cross-cutting replacive dunite bodies in the western block and smaller transposed and cross-cutting dunites in the eastern block is consistent with orthopyroxene dissolution by a percolating melt (Kelemen, 1990). For that reason, we suggest that the type-I orthopyroxene porphyroclasts in the harzburgites reflect the same melt-rock reaction leading to orthopyroxene 'corrosion' due to the melt-producing reaction:

orthopyroxene + low-Si melt → olivine + high-Si melt

Type-II orthopyroxenes (clusters of irregular grains with the same crystallographic orientations), are probably a more advanced stage of orthopyroxene replacement due to reaction with a melt.

The interstitial orthopyroxene in the fine-grained olivine–orthopyroxene domains surrounding orthopyroxene porphyroclasts (type-III orthopyroxene) in the eastern block tectonites may have a similar origin. The crystal orientation analysis in Fig. 8 shows that the crystal orientations of the fine-grained orthopyroxene are similar to that of the adjacent porphyroclast. It is unlikely that the fine-grained orthopyroxene is the result of dynamic recrystallisation of orthopyroxene porphyroclasts, since this process cannot explain the extensive mixing of olivine and orthopyroxene in the fine-grained domains. The melt-rock reaction invoked above to induce incongruent corrosion of orthopyroxene could explain the peculiar texture of the fine-grained domains. The irregular outlines of the porphyroclasts in the centres of the fine-grained domains suggest partial

replacement and growth of olivine grains at the expense of orthopyroxene. Suhr (1993) reported similar interstitial flaser-like orthopyroxene crystals in peridotites from the transition zone between harzburgites and massive dunites in the Bay-of-Island Ophiolite, also with the [*c*]-axes—the main orthopyroxene slip direction—at a high angle to the lineation. Suhr argues that "a formation of orthopyroxene due to corrosion (…) would be favoured from the geological context", but adopts an interpretation in which the small orthopyroxene crystals are derived from crystallisation from a trapped melt to account for the lattice preferred orientation and the morphology of the crystals (Suhr, 1993). In Othris, the fine-grained orthopyroxenes are probably residual, with their crystal orientations being inherited from the porphyroclast from which they were derived by corrosion. Their morphologies may be the result of stress-induced migration of olivine–orthopyroxene interphase boundaries (Wheeler, 1992) during deformation of the fine-grained domains.

A residual origin is not likely for the type-IV interstitial orthopyroxene in the olivine-rich domains in the fine-grained tectonites. Their presence along subgrain or low-angle grain boundaries within recrystallising olivine aggregates suggests that they precipitated locally during dynamic recrystallisation. As there are no orthopyroxene inclusions observed within preserved, unrecrystallised porphyroclasts, the option that such orthopyroxene crystals represent (relic) orthopyroxene inclusions within olivine porphyroclasts, which later controlled the location of subgrain boundaries developing within the olivine clast, can be rejected. Instead, it is suggested that the orthopyroxene crystals originated by precipitation from a melt migrating along grain edges defined by the intersections of subgrains and grain boundaries (cf. De Kloe, 2001), or by a replacement of olivine facilitated by diffusion of SiO_2 from nearby melt pockets into olivine crystals and recrystallising aggregates. It is difficult to envisage how a melt-absent, sub-solidus reaction could have produced the precipitation of orthopyroxene along low-angle boundaries. Such a reaction would probably have required a free fluid phase present along the grain boundaries to provide the necessary fast diffusion pathways into the recrystallising olivine crystals, for which—as mentioned above—evidence is absent in the rocks involved. Clearly, a melt-rock reaction, or at least a melt-facilitated reaction, is favoured to explain the observations. Together, type-III and type-IV orthopyroxene crystals point to a reaction with a melt that was probably close to orthopyroxene saturation and which was locally melt-forming and locally melt-consuming in the same rocks:

orthopyroxene + low-Si melt ↔ olivine + high-Si melt

Such a reaction implies that orthopyroxene existed at the liquidus of the melt that percolated though the Othris peridotites, which suggests that the melts had silica-rich, i.e. boninitic or ultra-depleted compositions (Dijkstra et al., 2001). Our optical analysis further suggests that orthopyroxene precipitation mainly occurred along (sub) grain boundaries sub-parallel to the foliation, while evidence for orthopyroxene corrosion is mainly observed on grain boundaries at a high angle to the foliation and in 'pressure-shadows' of large orthopyroxene clasts. This is suggesting that the direction of the reaction is dependent on (small) local variations in stress.

The development of straight, facet-like crystal faces on olivine grains adjacent to type-IV orthopyroxene grains is consistent with an origin by local orthopyroxene precipitation from a melt trapped in small grain boundary melt pockets. Many of these straight faces have orientations that coincide with low-index crystal faces (Fig. 10). The preference of (111), (021), and (110) faces agrees well with theoretical morphological models of (free) olivine growth, and these faces are frequently found in natural and artificial olivine crystals, whereas (121) is not uncommon ('t Hart, 1978b). The straight faces at low angles to, but not exactly coinciding with, the olivine (010) plane are more difficult to explain. They may be grain boundaries that only seem straight at light microscope resolution but which consist of a combination of stepping crystal faces at a smaller scale.

In summary, the tectonites of the western block exhibit evidence of dissolution of orthopyroxene, probably by a melt-rock reaction. In contrast, type-III and type-IV orthopyroxene crystals in the eastern block tectonites point to a more complex process of *dissolution and local precipitation* of orthopyroxene. The effect of this process in the tectonites of the eastern block is that orthopyroxene is re-distributed through the harzburgites, away from porphyroclasts into the olivine domains. Such a process requires a high mobility of the enstatite components, possibly due to high diffusion rates along (melt-wetted?) grain and subgrain edges. The process has led to the development of well-mixed fine-grained domains surrounding orthopyroxene porphyroclasts. The preservation of the fine grain sizes in these domains shows that olivine grain growth must have been very slow or even completely arrested, probably as the result of pinning of grain boundaries by interstitial orthopyroxene grains (cf. Olgaard, 1990).

5.4. Deformation in the mylonites and the cause of localisation

Field observations show that the fine-grained domains around orthopyroxene porphyroclasts in the tectonites of the eastern block become increasingly stretched when approaching the Onohonos River mylonite zone, until the fine-grained material forms continuous bands in the mylonite zone itself. The origin of the fine-grained bands in the mylonites can thus be traced back to the formation of the fine-grained rims around orthopyroxene porphyroclasts in the tectonites in the eastern block, and these tectonites can be seen as the protolith of the mylonites. This origin is also evident when the microstructures of mylonite samples are

studied: orthopyroxene porphyroclasts are restricted to the fine-grained bands, the fine-grained bands consist of a mixture of predominantly orthopyroxene and olivine, and the microstructures of the coarse-grained lenses strongly resemble those of the olivine bands in the eastern block tectonites.

The fine-grained domains in the eastern tectonites form isolated patches and the deformation of these tectonites was most likely controlled by the coarse-grained olivine-rich bands. In contrast, in the mylonites the deformation was probably controlled by the continuous and interconnected fine-grained bands. At thin section scale, coarse olivine-rich lenses are often boudinaged, suggesting that they acted as relatively strong layers in the weaker fine-grained matrix, which could flow around the stronger domains. This is confirmed by field observations showing that thin dunite bands are often broken-up or boudinaged. The absence of a (strong) LPO in the fine-grained bands rules out dislocation creep as the dominant deformation mechanism (Karato, 1988; Fliervoet et al., 1999). The presence of grain boundary alignments (Fig. 3c and d)—which are interpreted as sliding surfaces—in the fine-grained bands suggests that some grain boundary sliding occurred. However, an additional process must have been operating, adjusting the shapes of the grains to preserve the coherence of the crystal aggregate and prevent pores from opening. It is therefore most probable that the fine-grained bands deformed by a mechanism involving grain boundary sliding and diffusion creep. The apparent competency contrast between the fine-grained bands and the coarse-grained lenses and dunite layers is fully consistent with such a (grain-size sensitive) deformation mechanism.

Shear senses derived from the LPO patterns of the coarse olivine bands in the mylonites are ambiguous (with contrasting shear senses, even within the same sample, and double [*a*]-axis maxima). However, the coarse olivine bands in the mylonites are interpreted as remnants of the original tectonite structure, and their LPO was probably formed during tectonite deformation and unrelated to the deformation in the mylonite zone (and therefore, to the mylonite reference frame, i.e. foliation and lineation).

In conclusion we propose the following scenario for the formation of the mylonites. The first crucial step was the formation of fine-grained domains consisting of well-mixed olivine and orthopyroxene as the result of a reaction. The augen-shapes of the fine-grained domains in most of the tectonites show that they have been deformed to some extent during the deformation of the tectonites. The presence of an olivine LPO in the fine-grained domain in one tectonite may suggest that dislocation creep initially contributed to the deformation of the reaction-derived olivine. At some stage, however, the deformation mechanism in the fine-grained olivine must have switched completely to grain-size sensitive creep, probably during progressive cooling. With ongoing deformation of the tectonites, the domains became increasingly stretched until some of the domains coalesced to form continuous bands. From that stage onward, deformation locally became controlled by the weak fine-grained bands. As the deformation continued, an increasing number of fine-grained domains started to connect to form continuous bands. This process reduced the bulk strength of the peridotites with progressive deformation and led to strain localisation.

We thus argue that, in Othris, it was melt-rock reaction rather than dynamic recrystallisation that caused grain size reduction leading to a transition from dislocation creep to GSS creep. The well-mixed, polyphase character of the reaction-derived fine-grained domains was critical, as the presence of an interstitial phase (orthopyroxene) precluded grain growth of olivine, thus keeping the grain size small and allowing a switch to dominant GSS creep.

5.5. Temperature constraints

Pyroxene geothermometers of Bertrand and Mercier (1986), Brey and Köhler (1990) and Witt-Eickschen and Seck (1991) were used to constrain deformation temperatures. The chemical zonation of the pyroxenes shows that they re-equilibrated during cooling. The fact that Al in orthopyroxene shows a decrease from core to rim whilst the profile for Ca is relatively flat also shows that different elemental concentrations re-equilibrated to different extents due to variations in element diffusion rates. The single-pyroxene thermometer of Brey and Köhler, for instance, yields much lower temperatures (830–900 °C) when applied to the cores of the orthopyroxene porphyroclasts in the fine tectonite of Fig. 11 than the single-pyroxene thermometer of Witt-Eickschen and Seck (1000–1060 °C). The systematically lower temperatures obtained by the Brey and Köhler thermometer (which uses the Ca concentration in orthopyroxene) compared with those of the Witt-Eickschen and Seck thermometer (which uses Al) indicates that concentrations of Ca re-equilibrated more completely than those of Al during cooling. This is in agreement with the view that Ca diffusion is faster than Al diffusion in orthopyroxene (Witt-Eickschen and Seck, 1991). The two-pyroxene thermometers of Bertrand and Mercier (1986) and Brey and Köhler (1990), which are based on the exchange of Ca between co-existing clinopyroxene and orthopyroxene, also give low temperatures in the range of 800–860 and 725–800 °C for the cores of pyroxenes, confirming the extensive re-equilibration of Ca during cooling.

The analytical temperatures obtained by geothermometry reflect the temperatures at which the grains became closed for diffusive re-equilibration. The fact that fine-grained orthopyroxenes in the matrix of the studied samples are also zoned and that their Ca and Al concentrations plot on the same linear array as those of the porphyroclasts indicates that the fine-grained pyroxenes and the porphyroclasts have partly recorded the same cooling history. This means that the fine-grained orthopyroxene crystals must have formed

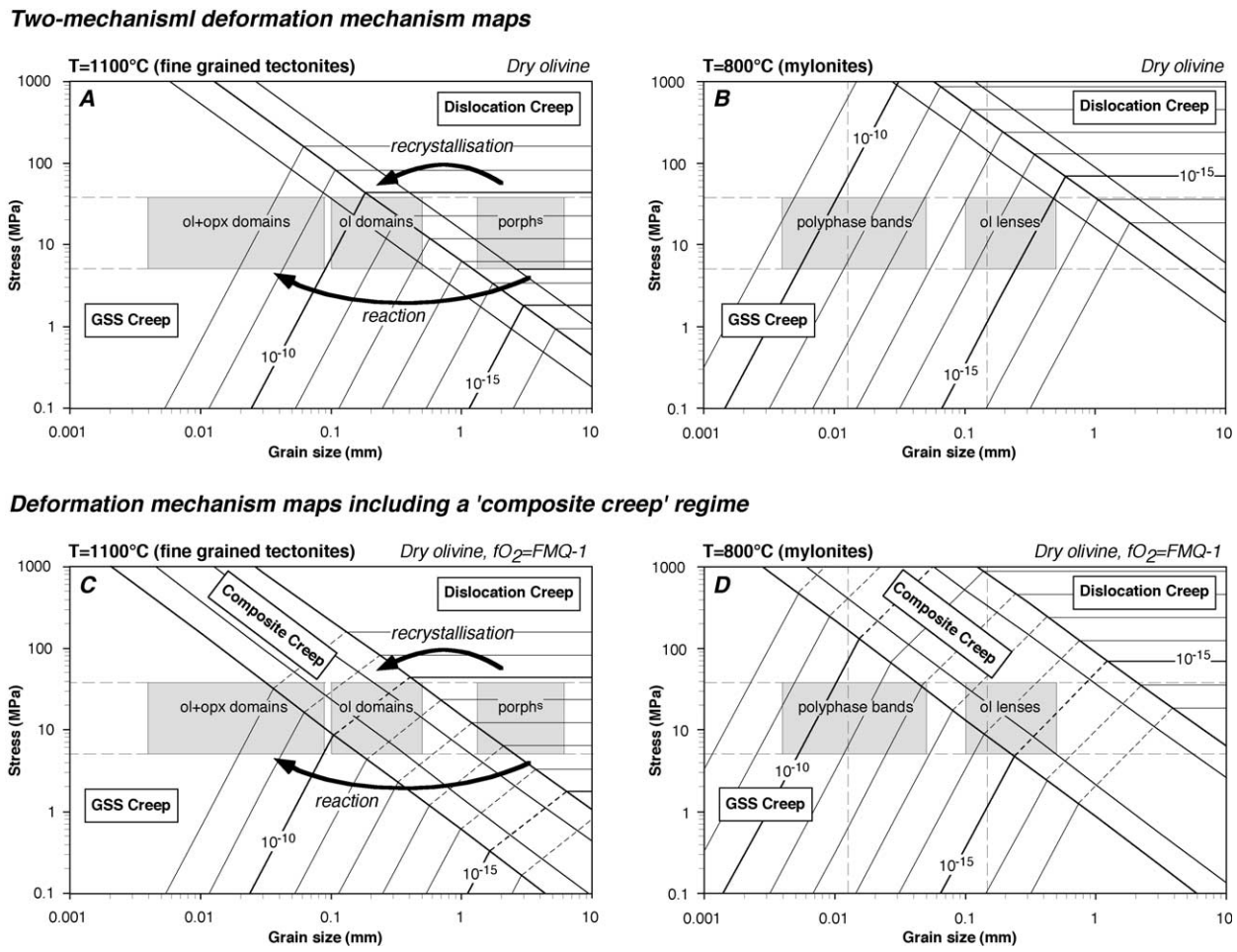

Fig. 13. Set of deformation mechanism maps for dry olivine (maps based on olivine flow laws shown in Table 1). (A) and (B) show two-mechanism maps indicating deformation conditions in the tectonites (temperature assumed as 1100 °C) and during mylonitic deformation at 800 °C. Thick lines running from top-left to bottom-right indicate conditions for 10, 50 and 90% dislocation creep (flow law of Chopra and Patterson, 1984). (C) and (D) show deformation mechanism maps for the same conditions that include a 'composite creep' regime, in which the deformation is controlled by GSS creep in combination with [*a*]-slip dislocation creep. Upper boundary of composite creep regime is defined by the (arbitrary) condition that the GSS creep rate is one tenth of the dislocation creep rate by [*c*]-slip; lower boundary is defined by the condition that GSS creep is 10 times faster than [*a*]-slip; other thick lines shown indicate equal contributions of GSS creep and [*a*]-slip, and GSS creep and [*c*]-slip. Flow laws for GSS creep and [*a*]-slip in (C) and (D) calculated for an oxygen buffer of FMQ-1. Thin lines are strain rate contours (in s^{-1}). The strain rates within the composite creep regime and their dependence on the grain size are unknown (depend, a.o., on whether GSS creep and [*a*]-slip occur in series or as parallel processes). Strain rate contours in this field are therefore drawn (dashed) by connecting the strain rate contours in the GSS field with those in the dislocation creep ([*c*]-slip]) field. Horizontal dashed lines are upper and lower stress estimates for fine tectonite deformation from paleopiezometry; grey boxes indicate grain size ranges in the pertinent domains (all grain sizes plotted are multiplied by 1.2 to correct for sectioning effects); vertical dashed lines in 800 °C diagrams are mean linear intercept grain sizes for olivine lenses and fine-grained polyphase bands in mylonites. The melt-rock reaction discussed in the text would have produced fine-grained material largely deforming in the GSS creep regime, while dynamically crystallised domains would have deformed (partly) by dislocation creep at much lower rates.

Table 1
Olivine flow laws used to construct deformation mechanism maps in Fig. 13. Strain rate is calculated as $d\epsilon/dt(s^{-1}) = A(fO_2/fO_2^{ref})^p \sigma^n d(m)^m \exp[-Q^{\#}/RT(K)]$; fO_2 is the relevant oxygen fugacity (FMQ-1 in this study), whereas fO_2^{ref} is the oxygen fugacity of the buffer used during the deformation experiment (Fe–FeO buffer for dislocation creep experiments, and Ni–NiO for GSS creep experiment). In Fig. 13c and d, olivine [*a*]-slip is assumed to take over from [*c*]-slip if GSS creep contributes more than 10% to the total deformation rate (corresponding to a relaxed Von Mises criterion), leading to a 'composite creep' regime ([*a*]-slip + GSS creep) in which the strain rate is grain size dependent (i.e. $m \geq 0$ for [*a*]-slip). See also Drury and Fitz Gerald (1998)

	A ($s^{-1}MPa^{-n}m^{p}$)	$Q^{\#}$ (J/mol)	n	m	p	Reference
Dry dislocation creep [*c*]-slip	2.88×10^4	5.35×10^5	3.6	0	0	Chopra and Patterson (1984); Drury and Fitz Gerald (1998)
Dry dislocation creep [*a*]-slip	2.48	3.85×10^5	3.5	≥ 0	0.33	Drury and Fitz Gerald (1998) and references therein
Dry GSS creep	2.46×10^{-10}	3.47×10^5	1.0	3	0.15	Hirth and Kohlstedt (1995a)

above their effective closure temperatures for the given chemical system. The closure temperature is dependent on the diffusion coefficient, the cooling rate, and the diffusion distance (Dodson, 1973; Spear, 1993). In geothermometry, the diffusion distance is effectively the distance to the rim of a mineral grain. Application of the Witt-Eickschen and Seck (1991) thermometer to the analyses of some of the largest (15–25 μm) orthopyroxene grains from fine-grained domains yields temperatures of 810–890 °C. These analyses represent the highest closure temperatures of the fine-grained orthopyroxene analysed and the analytical temperatures obtained are a minimum estimate of the temperature of the formation of the fine-grained orthopyroxene.

Another temperature constraint comes from the growth of tremolite + chlorite in the spaces between broken-up orthopyroxene fragments in plagioclase-bearing peridotite ultramylonite (Fig. 3g). The assemblage of calcic amphibole (tremolite) + chlorite is stable at temperatures below 780 °C in plagioclase–peridotites (Schmädicke, 2000). Therefore, at least some of the deformation in the mylonites occurred at temperatures below 780 °C.

5.6. Deformation mechanism maps

We constructed a set of two-mechanism deformation maps (see Frost and Ashby, 1982), based on experimentally-derived flow laws for dry olivine. We used the dislocation creep flow law of Chopra and Patterson (1984) and the diffusion creep flow law of Hirth and Kohlstedt (1995a). Fig. 13a shows such a two-mechanism map for a temperature of 1100 °C, which is thought relevant for the deformation of the tectonites and the formation of the fine-grained domains adjacent to orthopyroxene porphyroclasts. It is assumed that the protolith of the tectonites had an olivine grain size larger than 1 mm. Dynamic recrystallisation produced grains of 0.1–0.5 mm in the olivine domains, and the melt-rock reaction discussed above produced grains that were even smaller, down to sizes of a few microns. For stresses of 5–38 MPa, the grain size range found in the fine-grained domains falls entirely in the GSS creep field, which would suggest that the olivine LPO found in such a domain could not have been produced by dislocation creep. Moreover, according to the deformation mechanism map in Fig. 13a, dislocation creep would only have played a moderate role in the olivine domains, which is inconsistent with the widespread evidence for dislocation creep (substructure, LPO, dynamic recrystallisation) in these domains. Cooling to a temperature of 800 °C would have brought both the coarse olivine domains (corresponding to the olivine lenses in the mylonites) and the fine-grained domains (the polyphase bands in the mylonites) well into the GSS creep domain (Fig. 13b). Under these conditions, the fine-grained polyphase bands would have deformed up to four orders of magnitude faster than the coarser olivine lenses ($\sim 10^{-9}$–10^{-13} versus $\sim 10^{-13}$–10^{-16} s^{-1}). However, they would not have controlled the deformation in the tectonites because of their isolated (non-connected) character.

Recent deformation experiments have shown that under conditions close to the mechanism boundary between dislocation and GSS creep, the Von Mises criterion, which requires that the relatively strong [*c*]-slip system is activated during deformation of olivine polycrystals, is relaxed and that deformation is controlled by the weaker [*a*]-slip system under those conditions (see Hirth and Kohlstedt (1995b) and Drury and Fitz Gerald (1998) for discussion). This leads to another set of deformation mechanism maps, which include a 'composite creep' regime in which GSS creep in combination with [*a*]-slip controls the deformation (Fig. 13c and d). Within this domain the strain rate is grain size dependent as a result of the contribution of GSS creep. An 1100 °C deformation mechanism map, which includes such a composite creep regime (Fig. 13c) shows that dislocation creep ([*a*]-slip) would have played a role in the coarse olivine domains, and possibly in the coarsest material in the reaction-derived fine-grained olivine–orthopyroxene domains in the tectonites, which is in very good agreement with our microstructural observations. During cooling, the deformation mechanisms would have largely remained the same because the position of the lower boundary of the composite creep regime is only weakly temperature dependent as a result of the activation energies ($Q^{\#}$) for GSS creep and [*a*]-slip being very similar in magnitude (Drury and Fitz Gerald, 1998). Some dynamic recrystallisation could have reduced the maximum grain size in the well-mixed, reaction-derived olivine–orthopyroxene domains slightly, moving the polyphase bands in the mylonites completely into the GSS creep regime.

The deformation mechanism maps for the deformation rate in the mylonites at 800 °C shows that the strain rate in the olivine lenses was low, 10^{-13}–10^{-16} s^{-1}. Dynamic recrystallisation would therefore be slow, or arrested altogether, especially in the deformation mechanism map in Fig. 13b in which the olivine lenses lie completely in the GSS creep regime. The coarse granular domains consisting of polygonal olivine crystals, which are locally found within the olivine lenses in the mylonites (Fig. 3e) suggest that some grain growth and annealing occurred under these conditions. However, evidence for annealing is only found in olivine domains that do not contain (small amounts of) secondary phases along their grain boundaries. In contrast, the majority of the coarse bands contain very small amounts of orthopyroxene along olivine grain boundaries and they show no evidence for olivine annealing. This observation is consistent with the conclusion by Olgaard (1990) that even very small fractions of secondary phases, often just visible at the resolution of light microscopy, are sufficient to pin grain boundaries and can inhibit grain growth.

5.7. Implications for the strength of the mantle lithosphere

The case history of the Othris peridotite tectonites and

mylonites illustrates how a reaction possibly involving a melt can eventually lead to strain weakening, shear localisation, and mylonite formation. This study shows that not only sub-solidus reactions (e.g. Newman et al., 1999; Furusho and Kanagawa, 1999), but also melt-rock reactions can cause grain size reduction bringing olivine grains into the GSS creep field. The crucial issue is that the reaction produced small grains, and that it also led to intimate mixing of mineral phases, which inhibited grain growth, so as to preserve the fine grain sizes.

The ultimate effect of the process is extreme weakening. Strain rates in the fine-grained, reaction-derived bands in the Othris mylonites may have been several orders of magnitude faster than the strain rate in the coarse-grained, recrystallisation-derived olivine lenses (Fig. 13b and d). The weakness of the Othris mylonites is further illustrated by the plagioclase-bearing mylonites (Fig. 3h); the clast-like behaviour of plagioclase in the fine-grained polyphase matrix implies that the fine-grained matrix is weaker than the plagioclase clast. Such a microstructure shows that mantle rocks transected by fine-grained mylonites deforming by GSS creep can be weaker than rocks whose rheology is controlled by dislocation creep of plagioclase (e.g. lower crustal rocks). This suggests that under some conditions mantle rocks are weaker than lower crustal rocks, which is at variance with the commonly held perception that the shallow part of the mantle forms the strongest part of both the continental (e.g. Kirby, 1983; Kuznir and Park, 1986; Rutter and Brodie, 1988) and oceanic (Chen and Morgan, 1990; Shaw and Lin, 1996; see also Hirth et al., 1998 for discussion) lithosphere. The reduction of the bulk strength by the development of fine-grained mylonites can be of great importance to tectonic processes at ocean ridges. At magma-starved ocean ridges as well as during a-magmatic stages of seafloor spreading at slow-spreading ridges, spreading is accomplished by stretching of the oceanic lithosphere (Lin and Parmentier, 1989; Cannat, 1993, 1996; Tucholke and Lin, 1989; Escartin et al., 1997). Strength reduction due to the presence of peridotite mylonites may directly affect the rate of spreading in such settings. In addition, the structures and microstructures developed in the Othris massif show that during the onset of ophiolite emplacement, mylonite zones in the mantle may act as weak horizons along which slices of oceanic lithosphere may detach to eventually become emplaced as ophiolites.

6. Conclusions

Microstructural analysis of peridotite tectonites and mylonites in the Othris massif reveals a history of shear localisation that was associated with a change from dominant dislocation creep to grain-size sensitive (GSS) creep. The fine-grained olivine in the mylonite bands that deformed by GSS creep was produced by a reaction involving a melt, which led to the replacement of orthopyroxene porphyroclasts by a fine-grained mixture of olivine and interstitial orthopyroxene. The well-mixed character of this fine-grained material precluded olivine grain growth, thus keeping grain sizes small. Microstructures suggest that only tiny fractions of secondary minerals are sufficient to pin grain boundaries. Ongoing deformation led to elongation and, finally, coalescence of the fine-grained domains into a continuous network of mechanically weak, fine-grained, polyphase bands controlling the deformation.

Acknowledgements

Martin Menzies is thanked for suggesting the Othris Peridotite Massif as an interesting fieldwork area. Anna Rassios (IGME, Kozani) is thanked for support in Greece and for sharing some ideas and unpublished material on Othris. Ray Guillemette is thanked for his excellent supervision and assistance during the microprobe analyses at Texas A&M University. Further thanks go to Douwe Van Hinsbergen for providing fabric data of several Othris rocks, and to Gill Pennock for assistance with the SEM–EBSD. Thanks are due to the helpful people of Makrirahi, Smokovou, and Loutra Smokovou, for providing accommodation in their villages during several field seasons. This manuscript improved significantly as the result of the detailed reviews by Françoise Boudier and an anonymous reviewer. The work reported in this paper was mainly carried out at Utrecht University and was supported by NWO-PIONIER subsidy #030-75-346.

References

Bertrand, Ph., Mercier, J.-C.C., 1986. The mutual solubility of coexisting ortho- and clinopyroxene: toward an absolute geothermometer for the natural system? Earth and Planetary Science Letters 76, 109–122.

Boudier, F., Nicolas, A., 1995. Nature of the Moho transition zone in the Oman ophiolite. Journal of Petrology 36, 777–796.

Boudier, F., Ceuleneer, G., Nicolas, A., 1988. Shear zones, thrusts and related magmatism in the Oman ophiolite: initiation of thrusting on an oceanic ridge. Tectonophysics 151, 275–296.

Boullier, A.-M., Gueguen, Y., 1975. SP-mylonites: origin of some mylonites by superplastic flow. Contributions to Mineralogy and Petrology 50, 93–104.

Brey, G.P., Köhler, T., 1990. Geothermobarometry in four-phase lherzolites II. New thermobarometers, and practical assessment of existing thermobarometers. Journal of Petrology 31, 1353–1378.

Cannat, M., 1993. Emplacement of mantle rocks in the seafloor at mid-ocean ridges. Journal of Geophysical Research 98, 4163–4172.

Cannat, M., 1996. How thick is the magmatic crust at slow spreading ridges?. Journal of Geophysical Research 101, 2847–2857.

Ceuleneer, G., Nicolas, A., Boudier, F., 1988. Mantle flow patterns at an oceanic spreading centre: the Oman peridotites record. Tectonophysics 151, 1–26.

Chen, Y., Morgan, W.J., 1990. A nonlinear rheology for mid-ocean ridge axis topography. Journal of Geophysical Research 95, 17583–17604.

Chopra, P.N., Patterson, M.S., 1984. The role of water in the deformation dunite. Journal of Geophysical Research 89, 7861–7876.

De Bresser, J.H.P., Peach, C.J., Reijs, J.P.J., Spiers, C.J., 1998. On dynamic

recrystallization during solid state flow: effects of stress and temperature. Geophysical Research Letters 25, 3457–3460.

De Kloe, P.A., 2001. Deformation mechanisms and melt nano-structures in experimentally deformed olivine–orthopyroxene rocks with low melt fractions—an electron microscopy study. Ph.D. thesis, Utrecht University, Utrecht, The Netherlands, Geologica Ultraiectina 201, 173pp.

Dijkstra, A.H., 2001. Deformation and melt in natural mantle rocks: the Hilti Massif (Oman) and the Othris Massif (Greece). Ph.D. thesis, Utrecht University, Utrecht, The Netherlands, 164pp.

Dijkstra, A.H., Drury, M.R., Vissers, R.L.M., 2001. Structural petrology of plagioclase–peridotites in the West Othris Mountains (Greece): melt impregnation in mantle lithosphere. Journal of Petrology 42, 5–24.

Dodson, M.H., 1973. Closure temperature in cooling geochronological and petrological systems. Contributions to Mineralogy and Petrology 40, 259–274.

Drury, M.R., Fitz Gerald, J.D., 1998. Mantle rheology: insights from laboratory studies of deformation and phase transition. In: Jackson, I.N.S. (Ed.). The Earth's Mantle—Composition, Structure and Evolution. Cambridge University Press, pp. 503–559.

Drury, M.R., Hoogerduijn Strating, E.H., Vissers, R.L.M., 1990. Shear zone structures and microstructures in mantle peridotites from the Voltri Massif, Ligurian Alps, NW Italy. Geologie en Mijnbouw 69, 3–17.

Drury, M.R., Vissers, R.L.M., Van der Wal, D., Hoogerduijn Strating, E.H., 1991. Shear localization in upper mantle peridotites. Pure and Applied Geophysics 137, 439–460.

Escartin, J., Hirth, G., Evans, B., 1997. Effect of serpentinization on the lithospheric strength and the style of normal faulting at slow-spreading ridges. Earth and Planetary Science Letters 151, 181–189.

Etheridge, M.A., Wilkie, J.C., 1979. Grainsize reduction, grain boundary sliding and the flow strength of mylonites. In: Bell, T.H., Vernon, R.H. (Eds.), Microstructural Processes During Deformation and Metamorphism. Tectonophysics 58, pp. 159–178.

Fliervoet, T.F., Drury, M.R., Chopra, P., 1999. Crystallographic preferred orientations and misorientation in some olivine rocks deformed by diffusion or dislocation creep. Tectonophysics 303, 1–27.

Frost, H.J., Ashby, M.F., 1982. Deformation Mechanism Maps—the Plasticity and Creep of Metals and Ceramics. Pergamon Press, Oxford, New York.

Furusho, M., Kanagawa, K., 1999. Transformation-induced strain localization in a lherzolite mylonite from the Hidaka metamorphic belt of central Hokkaido, Japan. Tectonophysics 313, 411–432.

't Hart, J., 1978a. The structural morphology of olivine I. A qualitative derivation. Canadian Mineralogist 16, 175–186.

't Hart, J., 1978b. The structural morphology of olivine II. A quantitative derivation. Canadian Mineralogist 16, 547–560.

Hirth, G., Kohlstedt, D.L., 1995a. Experimental constraints on the dynamics of the partially molten upper mantle: deformation in the diffusion creep regime. Journal of Geophysical Research 100, 1981–2001.

Hirth, G., Kohlstedt, D.L., 1995b. Experimental constraints on the dynamics of the partially molten upper mantle. 2. Deformation in the dislocation creep regime. Journal of Geophysical Research 100, 15441–15449.

Hirth, G., Escartin, J., Lin, J., 1998. The rheology of the lower oceanic crust: implications for lithospheric deformation at mid-ocean ridges. In: Buck, W.R., Delaney, P.T., Karson, J.A., Lagabrielle, Y. (Eds.), Faulting and Magmatism at Mid-ocean Ridges. Geophysical Monograph 106, American Geophysical Union, pp. 291–303.

Hobbs, B.E., Mühlhaus, H.-B., Ord, A., 1990. Instability, softening and localization of deformation. In: Knipe, R.J., Rutter, E.H. (Eds.), Deformation Mechanisms, Rheology and Tectonics. Geological Society London Special Publication 54, pp. 143–165.

Hoogerduijn Strating, E.H., Rampone, E., Piccardo, G.B., Drury, M.R., Vissers, R.L.M., 1993. Sub-solidus emplacement of mantle peridotites during incipient oceanic rifting and opening of the Mesozoic Tethys (Voltri Massif, NW Italy). Journal of Petrology 23, 901–927.

Jaroslow, G.E., Hirth, G., Dick, H.J.B., 1996. Abyssal peridotite mylonites: implications for grain-size sensitive flow and strain localization in the oceanic lithosphere. Tectonophysics 256, 17–37.

Jin, D., Karato, S.-I., Obata, M., 1998. Mechanism of shear localization in the continental lithosphere: inference from the deformation microstructures of peridotites from the Ivrea zone, northwestern Italy. Journal of Structural Geology 20, 195–209.

Karato, S.-I., 1988. The role of recrystallization in the preferred orientation of olivine. Physics of the Earth and Planetary Interiors 51, 107–122.

Karato, S.-I., Wu, P., 1993. Rheology of the upper mantle: a synthesis. Science 260, 771–778.

Karato, S.-I., Toriumi, M., Fujii, T., 1980. Dynamic recrystallization of olivine single crystals during high-temperature creep. Geophysical Research Letters 7, 649–652.

Kelemen, P.B., 1990. Reaction between ultramafic rock and fractionating basaltic magma I. Phase relations, the origin of calc-alkaline magma series, and the formation of discordant dunite. Journal of Petrology 31, 51–98.

Kelemen, P.B., Dick, H.J.B., Quick, J.E., 1992. Formation of harzburgite by pervasive melt/rock reaction in the upper mantle. Nature 358, 635–641.

Kirby, S.H., 1983. Rheology of the lithosphere. Reviews of Geophysics and Space Physics 21, 1458–1487.

Kuznir, N.J., Park, R.G., 1986. Continental lithosphere strength: the critical role of lower crustal deformation. In: Dawson, J.B., Carswell, D.A., Hall, J., Wedepohl, K.H. (Eds.), The Nature of the Lower Continental Crust. Geological Society London Special Publication 24, pp. 79–93.

Lin, J., Parmentier, E.M., 1989. Mechanism of lithospheric extension at mid-ocean ridges. Geophysical Journal 96, 1–22.

Menzies, M., 1973. Mineralogy and partial melt textures within an ultramafic–mafic body, Greece. Contributions to Mineralogy and Petrology 42, 273–285.

Menzies, M., 1976. Rifting of a Tethyan continent—rare earth evidence of an accreting plate margin. Earth and Planetary Science Letters 28, 427–438.

Menzies, M., Allen, C., 1974. Plagioclase lherzolite—residual mantle relationships within two eastern Mediterranean ophiolites. Contributions to Mineralogy and Petrology 45, 197–213.

Newman, J., Lamb, W.M., Drury, M.R., Vissers, R.L.M., 1999. Deformation processes in a peridotite shear zone: reaction-softening by an H_2O-deficient, continuous net transfer reaction. Tectonophysics 303, 193–222.

Nicolas, A., Poirier, J.-P., 1976. Crystalline Plasticity and Solid State Flow in Metamorphic Rocks. John Wiley and Sons, London, UK 444pp.

Niu, Y., 1997. Mantle melting and melt extraction processes beneath ocean ridges: evidence from abyssal peridotites. Journal of Petrology 38, 1047–1074.

Olgaard, D.L., 1990. The role of second phase in localizing deformation. In: Knipe, R.J., Rutter, E.H. (Eds.), Deformation Mechanisms, Rheology and Tectonics. Geological Society London Special Publication 54, pp. 175–181.

Poirier, J.P., 1980. Shear localization and shear instability in materials in the ductile field. Journal of Structural Geology 2, 135–142.

Prior, D.J., Trimby, P.W., Weber, U.D., Dingley, D.J., 1996. Orientation contrast imaging of microstructures in rocks using forescatter detectors in the scanning electron microscope. Mineralogical Magazine 60, 859–869.

Prior, D.J., Boyle, A.P., Brenker, F., Cheadle, M.J., Day, A., Lopez, G., Peruzzo, L., Potts, G.J., Reddy, S.M., Spiess, R., Timms, N.O., Trimby, P.W., Wheeler, J., Zetterstrom, L., 1999. The application of electron backscatter diffraction and orientation contrast imaging in the SEM to textural problems in rocks. American Mineralogist 84, 1741–1759.

Randle, V., 1992. Microtexture Determination and its Applications. Institute of Materials, London 174pp.

Rassios, A., Konstantopoulou, G., 1993. Emplacement tectonism and

the position of chrome ores in the Mega Isoma peridotites, SW Othris, Greece. Bulletin of the Geological Society Greece XXVIII/2, 463–474.

Ross, J.V., Ave Lallemant, H.G., Carter, N., 1980. Stress dependence of recrystallized-grain and subgrain size in olivine. Tectonophysics 70, 39–61.

Rutter, E.H., 1999. On the relationship between the formation of shear zones and the form of the flow law for rocks undergoing dynamic recrystallization. Tectonophysics 303, 147–158.

Rutter, E.H., Brodie, K., 1988. The role of tectonic grain size reduction in the rheological stratification of the lithosphere. Geologische Rundschau 77, 295–308.

Schmädicke, E., 2000. Phase relations in peridotitic and pyroxenitic rocks in the model systems CMASH and NCMASH. Journal of Petrology 41, 69–86.

Shaw, W.J., Lin, J., 1996. Models of ocean ridge lithospheric deformation: dependence on crustal thickness, spreading rate, and segmentation. Journal of Geophysical Research 101, 17977–17993.

Spear, F.S., 1993. Metamorphic Phase Equilibria and Pressure–Temperature–Time Paths. Monograph Series 1. Mineralogical Society of America, Washington DC, 799pp.

Suhr, G., 1993. Evaluation of upper mantle microstructures in the Table Mountain massif (Bay of Islands ophiolite). Journal of Structural Geology 151, 1273–1292.

Tucholke, B.E., Lin, J., 1989. A geological model for the structure of ridge-segments in slow-spreading ocean crust. Journal of Geophysical Research 99, 11937–11958.

Twiss, R.J., 1977. Theory and applicability of a recrystallised grain size paleopiezometer. Pure and Applied Geophysics 115, 227–244.

Van der Wal, D., Chopra, P., Drury, M.R., Fitz Gerald, J.D., 1993. Relationship between dynamically recrystallised grain size and deformation conditions in experimentally deformed olivine rocks. Geophysical Research Letters 20, 1479–1482.

Vissers, R.L.M., Drury, M.R., Hoogerduijn Strating, E.H., Van der Wal, D., 1991. Shear zones in the upper mantle: a case study in an Alpine lherzolite massif. Geology 19, 990–993.

Vissers, R.L.M., Drury, M.R., Hoogerduijn Strating, E.H., Spiers, C.J., Van der Wal, D., 1995. Mantle shear zones and their effect on lithosphere strength during continental break-up. Tectonophysics 249, 155–171.

Vissers, R.L.M., Drury, M.R., Newman, J., Fliervoet, T.F., 1997. Mylonitic deformation in upper mantle peridotites of the North Pyrenean Zone (France): implications for strength and strain localization in the lithosphere. Tectonophysics 279, 303–325.

Wheeler, J., 1992. Importance of pressure solution and Coble creep in the deformation of polymineralic rocks. Journal of Geophysical Research 94, 145–159.

Wheeler, J., Prior, D.J., Jiang, Z., Spiess, R., Trimby, P.W., 2001. The petrological significance of misorientations between grains. Contributions to Mineralogy and Petrology 141, 109–124.

White, S.H., Knipe, R.J., 1978. Transformation- and reaction-enhanced ductility in rocks. Journal of the Geological Society London 135, 513–516.

White, S.H., Burrows, S.E., Carreras, J., Shaw, N.D., Humphreys, F.J., 1980. On mylonites in ductile shear zones. Journal of Structural Geology 2, 175–187.

Witt-Eickschen, G., Seck, H.A., 1991. Solubility of Ca and Al in orthopyroxene from spinel–peridotite: an improved version of an empirical geothermometer. Contributions to Mineralogy and Petrology 106, 431–439.

Zhang, S., Karato, S.-I., Fitz Gerald, J.D., Faul, U.H., Zhou, Y., 2000. Simple shear deformation of olivine aggregates. Tectonophysics 316, 133–152.